Magnetic Cell Manipulation and Sorting

Maciej Zborowski, Jeffrey J. Chalmers and William G. Lowrie

Abstract Cell manipulation is one of the fastest growing segments of biotechnology engineering, and magnetic cell separation plays a large part in its development. Because of low magnetic permeability of biological materials, the magnetostatic forces can be made to operate highly selectively on cells tagged with magnetic nanoparticles, with no interference from the physiological electrolyte solutions used for cell suspension and from other cells. The increasing availability of inexpensive permanent magnet blocks capable of generating fields in excess of 1 tesla (T) and gradients up to 1000 T/m combined with a large selection of targeting antibodies against nearly all cell surface markers of interest in clinical and laboratory applications, together with high-quality superparamagnetic iron oxide nanoparticles, makes magnetic separation an appealing alternative to other cell separation methods, including centrifugation and fluorescence-activated cell sorting. This chapter provides a brief overview of the underlying physical principles and a number of examples selected from a large body of scientific literature published on the subject.

M. Zborowski
Department of Biomedical Engineering, Lerner Research Institute,
Cleveland Clinic, Cleveland, OH, USA
e-mail: zborowm@ccf.org

J.J. Chalmers (✉) · W.G. Lowrie
Department of Chemical and Biomedical Engineering,
Analytical Cytometry Shared Resource, Comprehensive Cancer Center,
The Ohio State University, Columbus, OH, USA
e-mail: chalmers.1@osu.edu

© Springer International Publishing Switzerland 2017

W. Lee et al. (eds.), *Microtechnology for Cell Manipulation and Sorting*,
Microsystems and Nanosystems, DOI 10.1007/978-3-319-44139-9_2

Keywords Magnetophoresis · Magnetophoretic mobility · Magnetophoretic fractionation · Magnetic separation · Diamagnetic separation · Immunomagnetic separation · High gradient magnetic separator, HGMS · Magnetic field-flow fractionation · Particle tracking velocimetry · Cell tracking velocimetry · Biomagnetism · Biogenic magnetism · Cell magnetic susceptibility · Erythrocyte magnetic susceptibility · Intracellular paramagnetic species · Superparamagnetic iron oxide nanoparticles, SPIONs · Magnetic susceptibility-modified solutions · Magnetic nanoconveyors · Permanent magnet · Magnetic levitation

1 Introduction

Rapidly growing demands for better cell separation methods in cell biology and clinical laboratories propelled magnetic cell separation to the forefront of laboratory preparative separation techniques (Yavuz et al. 2009; Zborowski and Chalmers 2008; Pamme and Manz 2004). Its advantages include relative simplicity of operation, low capital investment, and rapidly expanding selection of targeting antibodies and magnetic tagging nanoparticles (Grützkau and Radbruch 2010). It has become one of the principal cell separation methods, alongside with centrifugation and fluorescence-activated cell sorting (FACS) (Gijs et al. 2010). Notable examples include its application to detection of rare, circulating tumor cells (CTCs) as a prognostic biomarker of cancer treatment approved by the U.S. Food and Drug Administration (FDA) for detection of metastatic breast, prostate, and colorectal CTCs (de Wit et al. 2015). Progress in the chemistry of superparamagnetic iron oxide nanoparticles (SPIONs) and their conjugation with monoclonal antibodies made it possible to sort cells in high throughput bioassays (Vyas et al. 2012). Notable recent examples include ligand-independent magnetic cell sorting by field-induced cell motion (magnetophoresis) instead of capture on a solid substrate (Karabacak et al. 2014). This, plus a rapid progress in microelectromechanical systems (MEMS), optical detection and separation technologies brought about much improved understanding of CTC biology. The remarkable increase in the strength of permanent magnets over the past two decades makes it possible to consider building a practical system strong enough to sort cells based on their weakly paramagnetic moment, without labeling by SPIONs (Knowlton et al. 2015; Sumari et al. 2016; Melnik et al. 2007). This chapter provides a brief review of underlying physical principles of magnetic cell separation and selected examples that only partially cover the rapidly expanding field.

2 Elements of Magnetostatics in Application to Cell Separation

The unique feature of magnetic cell separation is that it is performed in a continuous phase (aqueous electrolyte solutions) that is similar in its characteristic physical properties to those of the dispersed phase (cells) because of the cells' high water content (approximately 70 % volume by volume, v/v). This is unlike magnetic separation in typical industrial applications, such as separation of iron contaminants from dry mass or iron particles from environmental water, or use of magnetic forces in particle physics requiring high vacuum (Ramsey 1990; Sun 1980). The similarity between the continuous and dispersed phases poses challenges in magnetic cell separation but is also a source of opportunities that continue to be explored in many laboratories. Therefore, a brief overview of the magnetic forces and their effect on cell motion in the viscous media is provided here.

2.1 Magnetic Ponderomotive Force in Two-Phase Media

The application of the magnetic field to an aqueous cell suspension leads to the magnetic polarization (magnetization) of both the dispersed phase (cells) and the continuous phase (aqueous electrolyte solution). The resulting local field causing the cell magnetization is modified by the magnetization of the continuous phase, resulting in the expression for the force similar to that describing the effect of the dielectric polarization on the local electric field, known as Clausius–Mossotti relation (Schwinger et al. 1998). Thus assuming a small, spherical, magnetically polarizable particle of radius R and magnetic permeability μ_p free to translate and rotate in magnetically polarizable solution of magnetic permeability μ_s, the magnetic force acting on the particle is

$$\mathbf{F}_m = 4\pi R^3 \frac{\mu_p - \mu_s}{\mu_p + 2\mu_s} \mu_s H \nabla B, \tag{1}$$

where H is the local magnetic field strength (in ampere/m, A/m) and ∇B is the gradient of the magnetic field induction B (in tesla, T) measured in the absence of the magnetically polarizable media. Here the dimensionless, relative magnetic permeabilities are used, expressed with respect to the magnetic permeability of free space, $\mu_o = 4\pi \times 10^{-7}$ T m/A. For a freely suspended particle, the magnetic force vector is thus aligned with the vector of the local field gradient. It vanishes in the absence of the local field gradient. For separation of small, weakly magnetizable particles, high magnetic field gradients are necessary.

Related to the molecular properties of the magnetically polarizable materials, their relative magnetic permeability differs from slightly less than unity (diamagnetic matter, such as water) to more than unity (paramagnetic matter) to several orders of magnitude higher than unity (ferromagnetic materials). This has

interesting implications for the direction of the magnetic force vector relative to that of the local field gradient as that direction depends on the sign of magnetic permeability difference, $\mu_p - \mu_s$. Thus, six combinations are possible:

1. Paramagnetic particle in weakly paramagnetic solution, $1 < \mu_s < \mu_p \rightarrow \mu_p - \mu_s > 0$ resulting in the magnetic force being parallel to the local field gradient (attractive force).
2. Weakly paramagnetic particle in a (relatively) strongly paramagnetic solution, $1 < \mu_p < \mu_s \rightarrow \mu_p - \mu_s < 0$ resulting in the magnetic force being antiparallel to the local field gradient (repulsive force).
3. Paramagnetic particle in diamagnetic solution, $0 < \mu_s < 1 < \mu_p \rightarrow \mu_p - \mu_s > 0$ (attractive force).
4. Diamagnetic particle in paramagnetic solution, $0 < \mu_p < 1 < \mu_s \rightarrow \mu_p - \mu_s < 0$ (repulsive force).
5. Diamagnetic particle in a relatively weaker diamagnetic solution, $0 < \mu_p < \mu_s < 1 \rightarrow \mu_p - \mu_s < 0$ (repulsive force).
6. Diamagnetic particle in a relatively stronger diamagnetic solution, $0 < \mu_s < \mu_p < 1 \rightarrow \mu_p - \mu_s > 0$ (attractive force).

All six instances of the attractive and repulsive magnetic forces have been described in the literature on magnetic cell separation, leading to interesting observations of the fundamental and practical nature. One of them was an apparent contradiction with the fundamental tenet of magnetostatics that the magnetostatic forces alone (or in combination with conservative forces, such as gravity) could not lead to a stable equilibrium (the Earnshaw theorem applied to magnetostatics). A vivid illustration is an everyday life experience of impossibility of suspending a steel ball in the air using permanent magnets only. Yet such a stable configuration has been realized by replacing air with a ferrofluid of a higher magnetic permeability than that of the steel ball (which would make it an example of the type no. 2 in the above list, with the paramagnetic matter replaced by the ferromagnetic one) (Rosensweig 1997). Practical examples of type 4 in the list include addition of soluble paramagnetic ions (rare earth) to separate dispersed phase (such as cells) by magnetic repulsion (Zimmels and Yaniv 1976; Watarai and Namba 2001; Moore et al. 2004; Peyman et al. 2009; Hwang et al. 1984). Other examples include magnetic attraction of deoxygenated erythrocytes as a type 6 mechanism, and magnetic repulsion of oxygenated erythrocytes as type 5 mechanism (albeit very weak in typical laboratory applications) (Zborowski et al. 2003).

Most magnetic permeabilities encountered in the biological magnetic separations are small, with their relative permeabilities very nearly equal to unity, and therefore their magnetic properties are more conveniently described by the volume magnetic susceptibility, $\chi = \mu - 1$. From the foregoing, $\chi > 0$ for paramagnetic and ferromagnetic materials, and $\chi < 0$ for diamagnetic materials. With the substitution of $\mu = \chi + 1$ in Eq. (1), one obtains:

$$\mathbf{F}_m = 4\pi R^3 \frac{\chi_p - \chi_s}{\chi_p + 2\chi_s + 3}(\chi_s + 1) H \nabla B \quad \overset{\chi_p \ll 1,\, \chi_s \ll 1}{\longrightarrow} \quad \frac{4}{3}\pi R^3 \left(\chi_p - \chi_s\right) \tag{2}$$

The limiting case for $\chi_p \ll 1$, $\chi_s \ll 1$ shown on the right approximates well most if not all the magnetic cell separation situations, where the volume magnetic susceptibility of the particle (cell) and the aqueous electrolyte solution is orders of magnitude smaller than unity (the volume magnetic susceptibility of water is $\chi_{H_2O} = -9.05 \times 10^{-6}$). Further simplification is obtained if one assumes that the direction of the magnetic field gradient, ∇B changes little along the particle (cell) trajectory, in which case only the force in the direction of the dominant component of the field gradient is considered, here along the $0x$ axis:

$$F_m = \frac{4}{3}\pi R^3 (\chi_p - \chi_s) H \frac{dB}{dx}. \tag{3}$$

The above formula is the one most frequently encountered in the literature on magnetic cell separation for the good reason of providing a satisfactory, quantitative measure of the magnetic force on the cell based on the material properties of the cell and the continuous phase, and the imposed, local magnetic field and gradient (unperturbed by the media). There are other forms of the same equation of the magnetic force on a cell whose usefulness depends on the context. One particular variant often encountered in the literature makes an explicit use of the cell volume, $V = \frac{4}{3}\pi R^3$ and the fact that the magnetic permeability of the media is practically equal to that of the free space, so that $H = \frac{B}{\mu_0}$ and therefore $H\frac{dB}{dx} = \frac{d}{dx}\left(\frac{B^2}{2\mu_0}\right)$ leading to the expression:

$$F_m = V(\chi_p - \chi_s)\frac{d}{dx}\left(\frac{B^2}{2\mu_0}\right) \tag{4}$$

which emphasizes the fact that the magnetic force is proportional to the gradient of square of the local field magnitude, for materials whose magnetization is a linear function of the applied field (diamagnetic and paramagnetic). The importance of the field variable $\frac{B^2}{2\mu_0}$ (where μ_0 is a constant) is that it has a dimension of the magnetostatic energy density (in J/m^3) which allows a direct comparison of magnetic force generation by permanent magnets, such as used for magnetic separation, typically characterized by the (external) field energy product given in units of megagauss × oersted, MGOe, equivalent to 7957.75 J/m^3 in the SI system. Thus the neodymium–iron–boron (NdFeB) magnet rated at the energy product of 50 MGOe (3.98×10^5 J/m^5) has a capability of exerting a force on paramagnetic or superparamagnetic substance that is up to 100 times higher than that of an Alnico magnet rated at five MGOe (assuming the same geometrical magnet configuration and no demagnetization effects). Another important property of the field variable $\frac{B^2}{2\mu_0}$ is that it has a dimension of pressure (in pascals) and as such plays an important role in magnetohydrodynamics and ferrohydrodynamics, where it is referred to as the magnetic field pressure (Rosensweig 1997). Thus Eq. (4) provides a link between the magnetohydrodynamics and a special case of the magnetic force on discrete particles (cells) in continuous media.

2.2 Note on the Magnetic Susceptibility

There are a bewildering number of definitions of the magnetic susceptibility encountered in the scientific literature, reflecting the depth and width of research and applications of the electromagnetic phenomena, and a nearly 200 year history of rigorous, quantitative materials' property determinations. The task of recalculating one type of magnetic susceptibility to another could be quite daunting, especially to a novice to the magnetic cell separation literature, yet necessary for any meaningful comparison between various magnetic separation systems. A brief summary of the most frequently used formulas is provided below. The problem is compounded by different systems of units used in the literature, which further complicates an effective communication in such an interdisciplinary field that is magnetic cell separation. The comparison between the two most relevant systems of unit important for the magnetic separation topic, electromagnetic Gauss system of units (centimeter–gram–second–coulomb, EM CGS), and the International System of units (meter–kg–second–ampere, MKSA, or SI) is illustrated in Table 1. The SI system of units is used in this chapter.

2.2.1 Volume Magnetic Susceptibility

The susceptibility χ used in Eq. (3) is the volume magnetic susceptibility. It has the desirable feature of being a dimensionless quantity and a simple physical interpretation as a ratio of the magnetization of matter (more on magnetization below), M, to the imposed magnetic field in the absence of matter, H:

$$\chi = \frac{M}{H}. \tag{5}$$

Both M and H are in the units of Å/m. The volume magnetic susceptibility is the standard magnetic susceptibility in the physics literature and is occasionally referred to simply as the magnetic susceptibility.

Table 1 Magnetic susceptibility conversion factors

Susceptibility designation	Symbol	χ (EMU CGS units)	χ (SI units)	To obtain value in SI units, multiply value in EMU CGS units by
Volume	χ	1	1	4π
Mass	χ_g	$\frac{cm^3}{g}$	$\frac{m^3}{kg}$	$\frac{4\pi}{1000}$
Specific	χ_g	$\frac{cm^3}{g}$	$\frac{m^3}{kg}$	$\frac{4\pi}{1000}$
Molar	χ_N	$\frac{cm^3}{mol}$	$\frac{m^3}{mol}$ or $\frac{m^3}{kmol}$	$\frac{4\pi}{10^6}$ or $\frac{4\pi}{1000}$, respectively
One-gram-formula-weight	χ'_N	$\frac{cm^3}{mol}$	$\frac{m^3}{mol}$ or $\frac{m^3}{kmol}$	$\frac{4\pi}{10^6}$ or $\frac{4\pi}{1000}$, respectively

2.2.2 Mass (or Specific) Magnetic Susceptibility

The mass magnetic susceptibility, χ_g, arises when the volume of substance is replaced by its mass in Eq. (1), as is the case in many practical applications for which it is easier to determine the mass (by way of the weight) than the volume of substance, such as for dry matter. The conversion of the mass magnetic susceptibility to volume magnetic susceptibility requires determination of the mass density, ρ of the substance:

$$\chi = \chi_g \rho \tag{6}$$

The unit of the mass (or specific) magnetic susceptibility is the inverse of the mass density, $[\chi_g] = \mathrm{m}^3/\mathrm{kg}$.

2.2.3 Molar Magnetic Susceptibility

The molar magnetic susceptibility, χ_N arises from measurements of known molar amounts of the substance, and in order to recalculate it to the standard volume magnetic susceptibility, a known molar concentration, c_N (molarity, in units of mol/L) is required:

$$\chi = \chi_N c_N \times 1000, \tag{7}$$

where the factor 1000 accounts for the conversion of the molarity, c_N, to mol/m^3. The unit of the molar magnetic susceptibility typically encountered in the literature is L/mol, and in the proper SI units it is $[\chi_N] = \mathrm{m}^3/\mathrm{mol}$.

2.2.4 One-Gram-Formula-Weight Magnetic Susceptibility

The one-gram-formula-weight susceptibility, χ'_N also arises from measurements of known molar amounts, but unlike the molar magnetic susceptibility, the mass and the volume of the substance are required to recalculate it to the standard volume magnetic susceptibility. For known mass density, ρ and the molecular weight, M_w of the substance, one obtains:

$$\chi = \chi'_N \frac{\rho}{M_w} \tag{8}$$

Again, care is required to express ρ and M_w in the SI units (kg/m^3 and kg/mol) rather than the customary CGS units (g/cm^3 and g/mol). The units of the one-gram-formula-weight magnetic susceptibility are the same as the molar susceptibility, $[\chi'_N] = \mathrm{m}^3/\mathrm{mol}$. The significance of this type of magnetic susceptibility is that it is occasionally used in the reference books in physics and chemistry, a carryover from older literature.

2.2.5 Magnetic Susceptibility of a Mixture (or Bulk Magnetic Susceptibility)

For a compound substance, the volume magnetic susceptibility is the weighted sum of the component susceptibilities, with the volume fraction as the weighting factor:

$$\chi = \sum_{i=1}^{N} \phi_i \chi_i, \tag{9}$$

where χ_i is the volume magnetic susceptibility of the ith component with the fractional volume of $\phi_i = V_i/V$, $i = 1 \ldots, N$ and V is the total volume of the sample.

2.2.6 Magnetic Susceptibility Conversion Factor Between the CGS and SI System of Units

For the properly defined volume magnetic susceptibilities in the two units systems, the conversion factor is 4π, so that the susceptibility in the SI units is 4π-times larger than that in the CGS units. For instance, water volume susceptibility (CGS) is -0.72×10^{-6}, that in the SI system of units (SI) is -9.04×10^{-6}.

3 Basic Magnetic Properties of Matter

The introduction of matter in the magnetic field modifies the field and the difference between the field measured in the matter, **B** and the field in free space, **H** is the matter magnetization:

$$\mathbf{M} = \frac{\mathbf{B}}{\mu_0} - \mathbf{H} \tag{10}$$

Here again the constant μ_0 is the unit conversion factor. In the absence of matter (in free space) or for very weakly magnetized substances ($|M| \approx 1$ A/m) typical of air, water and applications in biology, magnetization vanishes or is assumed negligible and the B field equals the H field, $\mathbf{B} = \mu_0 \mathbf{H}$. For strongly magnetic materials, the magnetization may far exceed the applied field H, often by several orders of magnitude (iron). Because of the difference in the response to the applied magnetic field, the materials are classified as (1) diamagnetic, weakly magnetized in the opposite direction to the applied field, (2) paramagnetic, moderately magnetized in the direction of the applied field, and (3) ferromagnetic, strongly magnetized in the direction of the applied field. The magnetic properties of matter are directly related to its molecular composition and the topic far exceeds the scope of this chapter. There are many excellent introductory tests and advanced textbooks covering various aspects of the magnetic properties of matter (Jiles 2016).

Suffices to say that magnetic materials are at the heart of the key technologies of modern life, including information technology (hard disk drives and mass information storage), microwave ovens (based on magnetron), reusable energy technology (wind turbines), electric cars, and small electric helicopters (drones) just to name the few. Closer to the topic of this chapter, the rapid progress in the synthesis and characterization of magnetic microparticles and nanoparticles made it possible to design and implement new, high sensitivity diagnostic tests, MRI contrast agent, targeted hyperthermia for localized tumor treatment, and the magnetic cell separation (Jiles 2016; Krishnan 2016). Therefore, the topic of material magnetization will be treated here only briefly, focusing on the aspects important for magnetic cell separation.

3.1 Linearly Magnetizable Matter

A linear relationship between the magnetization and the applied field is characteristic of diamagnetic and paramagnetic substances, with the volume magnetic susceptibility as a proportionality constant, χ (Eq. 5). The diamagnetic substances are repulsed by the magnetic field and the paramagnetic substance is attracted by it, as already mentioned above. Illustrative examples are discussed below.

3.1.1 Diamagnetic Matter

The diamagnetism is present in all types of substances because it is related to subatomic properties of matter. For relatively weak magnetic fields, its presence is negligible and in the presence of paramagnetic and ferromagnetic effects, it is usually masked by them because it is the weakest of the three. Nevertheless, for accurate susceptibility determination, the diamagnetic contributions from the sample constituents cannot be neglected, especially if those constituents take up a significant volume fraction of the sample (Eq. 8), such as water in the cell (70 % v/v or higher). For sufficiently high magnetic fields and gradients, the diamagnetic effects become appreciable and have been proposed for use in practical applications, such as diamagnetic separation (Peyman et al. 2009; Hirota et al. 2004; Mirica et al. 2009, 2010; Vojtisek et al. 2012). To estimate the magnitude of the magnetic field and gradient necessary to suspend a water droplet in the air, one compares the magnetic force (Eq. 4) to the weight ($\rho V g$) of the droplet:

$$\frac{F_\mathrm{g}}{F_\mathrm{m}} = \frac{\rho V g}{\chi^V \frac{\mathrm{d}}{\mathrm{d}x}\left(\frac{B^2}{2\mu_0}\right)} = \frac{\rho}{\chi} \cdot \frac{2\mu_0 g}{\frac{\mathrm{d}B^2}{\mathrm{d}x}} \quad \overset{F_\mathrm{m}=F_\mathrm{g}}{\longrightarrow} \quad \frac{\mathrm{d}B^2}{\mathrm{d}x} = 2\mu_0 g \frac{\rho}{\chi}, \tag{11}$$

where $\rho = 1000\ \mathrm{kg/m^3}$ is the water mass density, $g = 9.81\ \mathrm{m/s^2}$ is the standard gravitational acceleration, $\chi = -9.05 \times 10^{-6}$ and $\mu_0 = 4\pi \times 10^{-7}\ \mathrm{T\,m/A}$. Note that the volume V of droplet dropped out of the equation. No correction for the

air density and air magnetic susceptibility was made in Eq. (11). The resulting field energy density gradient required to suspend the water droplet in the air is 2720 T^2/m, which could be achieved, for instance, in a configuration of field gradient of 272 T/m and field magnitude of 10 T. This has been experimentally demonstrated using superconducting magnets (Hirota et al. 2004) and is within the reach of permanent magnets and microdroplets, for which the field gradients could be made much higher to compensate for the lower available magnetic field, for instance 1500 T/m and field of 1.82 T.

The majority of biological material is diamagnetic with a few important exceptions, such as hemoglobin and its derivatives (Zborowski et al. 2003), ferritin (Zborowski et al. 1995), magnetosomes in magnetotactic bacteria (Posfai et al. 2013), and endospores of *Bacillus thuringiensis* (Melnik et al. 2007). The bulk magnetic susceptibility of eukaryotic organisms is diamagnetic as demonstrated by magnetic levitation of whole organisms, notably frogs and strawberries (Simon and Geim 2000).

3.1.2 Paramagnetic Matter

Unlike diamagnetic matter, paramagnetic matter consists of atomic or molecular permanent magnetic dipoles whose magnitude does not depend on the applied magnetic field, in particular, they do not vanish in the absence of the magnetic field. Rather, their spatial orientation depends on the magnetic field—the higher the field, the higher the degree of alignment with the local field vector. The unit atomic dipole moment is Bohr magneton, $\mu_B = 9.274 \times 10^{-24}$ J/tesla (J/T). A good first approximation of the net magnetization of a mole of paramagnetic material per unit of the applied magnetic field is that of an ideal gas of elementary magnetic dipoles, μ_A at the absolute temperature T, due to Paul Langevin (Bozorth 1993). In the limit of low field, the molar magnetic susceptibility does not depend on the applied field and is a quadratic function of the elementary magnetic dipole moment, μ_A and an inverse function of the temperature:

$$\chi_N = \frac{N_A \mu_0 \mu_A^2}{3kT}, \tag{12}$$

where $k = 1.38 \times 10^{-23}$ J/kelvin (J/K) is the Boltzmann constant and $N_A = 6.022 \times 10^{23}$ is the Avogadro number. With increasing applied field the molar magnetization departs from linearity and it becomes a (Langevin) function of the applied field, reaching saturation at high fields. Further refinements include correction to temperature T by replacing it by $T - T_C$, where T_C is the Curie temperature below which the elementary dipole moments become frozen in space, important in the description of ferromagnetic materials (see below). Quantum mechanical effects are introduced by replacing Boltzmann statistics of the elementary dipole moment distribution by quantized states statistics limiting the number of allowable dipole orientations relative to the applied field vector (due to Brillouin) (Bozorth 1993). This was used by Pauling and Coryell (1936) to

demonstrate consistency of the quantum mechanical model of chemical bond with experimental measurements of the magnetic susceptibility using hemoglobin and its derivatives as an example.

Examples of paramagnetic substances include certain lanthanides and their aqueous solutions. For instance, gadolinium has the fourth highest magnetic moment of all the elements (7.95 Bohr magnetons), significantly higher than elemental iron (2.2 Bohr magnetons) (Bozorth 1993). Correspondingly, the molar susceptibility of Gd^{3+} is 0.34 in room temperature. The high magnetic moment, plus the extreme stability of the Gd–DTPA complex, made it a contrast agent of choice for MRI applications. Commercial preparations of chelated gadolinium, such as Magnevist (Berlex Labs, Richmond, CA, USA) and Optimark (Mallinckrodt Inc., St. Louis, MO, USA) were used but had to be withdrawn from the market because of kidney toxicity. The strictly paramagnetic behavior of lanthanide solutions is important for calibration of the instruments used for measuring cell magnetophoresis by cell tracking velocimetry (CTV) (Moore et al. 2004; Zhang et al. 2005). Paramagnetic solutions of erbium have been evaluated for use as the cell magnetization reagents for magnetic cell separation (Russell et al. 1987; Zborowski et al. 1992).

Another example of paramagnetic compound important in the context of magnetic cell separation is hemoglobin, the oxygen-carrying protein in red blood cells. The paramagnetic contribution comes from the heme group but not from the globin part, and only when the hemoglobin is dissociated from the oxygen molecule (deoxyhemoglobin). The effective magnetic moment of the deoxy heme group is 5.46 Bohr magnetons, and the total paramagnetic contribution of the heme increases to four times that value because of the presence of four heme groups in the hemoglobin molecule. With the binding of the oxygen molecule, the electronic structure of the heme group changes so that its magnetic dipole moment vanishes (Pauling and Coryell 1936). The paramagnetic forces acting on deoxygenated erythrocytes are sufficiently high to observe their motion in the magnetic field (Zborowski et al. 2003).

3.2 Superparamagnetic Microparticles

The atomic structure of certain metals, notably iron, favors coordination of elemental magnetic dipole moments below Curie temperature over the distances of hundreds of atom diameters. The effect is known as the ferromagnetism (Jiles 2016; Bozorth 1993). This gives rise to a strong magnetization of the volume of such coordinated magnetic moments, known as the magnetic domain (Jakubovics 1994). The magnetic properties of ferromagnets depend, among other things, on their size. In particular, if the size of a ferromagnetic material is equal to or smaller than that of a magnetic domain, typically on the order of 10 nm, then such materials are extremely hard to demagnetize and behave like single but large magnetic dipoles (Krishnan 2010). The magnetic moment of such magnetic domain

dipoles can reach 10^5 Bohr magnetons (Gider et al. 1995). The collective behavior of such nanoparticles, including the volume magnetization of their liquid suspension, is similar to that of paramagnetic solutions except that it is much stronger (Rosensweig 1997). In particular, the magnetization curve of a superparamagnetic colloid does not depend on previous history of magnetization (no hysteresis) and ideally crosses zero. For that reason such a dispersed phase came to be known as "superparamagnetic". Superparamagnetic particles have many interesting properties and are a subject of active research and applications. In particular, because of their small size and high magnetic moment, and in the case of iron, relatively low toxicity, they are an ideal component of magnetic cell separation schemes. That particular class of magnetic particles is often referred to as "superparamagnetic iron oxide nanoparticles", or SPIONs, in the magnetic cell separation literature (Thanh 2012). All commercial magnetic cell separation systems operate on the basis of selective attachment of superparamagnetic particle to target cells and their removal from suspension by the applied magnetic field. From Eqs. (4), (7), (9), and (12), and for known composition and physical properties of SPIONs one calculates that it takes only a few SPIONs to convert the average volume magnetic susceptibility of the cell–SPION complex from diamagnetic to paramagnetic and thus isolate it magnetically from an aqueous suspension of unlabeled cells. The high specificity of SPIONs to a particular cell type is achieved by conjugating it to a ligand such as a monoclonal antibody that has high specificity to that particular cell type (Grützkau and Radbruch 2010). SPION suspensions have other biomedical uses, such MRI contrast agents, replacing chelated gadolinium solutions because of their lower toxicity. They have been considered for applications to tumor-targeted hyperthermia although their mechanism of action is unclear because they lack hysteresis and therefore do not dissipate demagnetization energy. They gave rise to a new body imaging technique, termed "Magnetic Particle Imaging" (MPI) that provides information about SPION distribution in the body similar to the information provided by an MRI contrast agent but at a much lower cost of the capital equipment as no large, superconducting MRI magnets are required but only a set of Helmholtz coils for the imaging (Krishnan 2016). The preparation of magnetic particles for biomedical applications, including cell separation has to take into account not only the magnetic properties of the particle, but also its biological activity, including toxicity and biocompatibility (Hafeli et al. 2008).

3.3 Ferromagnetism and Permanent Magnets

Large, multi-domain structures in the order of centimeters form permanent magnets that have been known since antiquity. They gave the name to the science of magnetic phenomena, thought to be derived from an ancient site of the magnetic mineral mining in Turkey's Aegean Region. The mineral, magnetite, consists of a mixture of iron oxides at different oxidation states, 2+ and 3+, with the chemical

formula designated as Fe_3O_4. The synthesis and characterization of permanent magnet materials is a very active part of materials science and engineering, and the magnetic field intensity generated by the permanent magnet has grown exponentially since 1940s. Because their magnetic properties are qualitatively comparable to those of the natural magnetic mineral consisting of iron oxide, they are classified as "ferromagnets" and the associated phenomena as "ferromagnetism". Pure metallic iron, Fe is ferromagnetic up to its Curie temperature of 770 °C, above which it becomes paramagnetic (Bozorth 1993). In addition to iron, cobalt and nickel also exhibit ferromagnetic properties, and are used in combination with iron, as alloys, for permanent magnet production (Al–Ni–Co, or Alnico). The current, widely used commercial magnets are alloys of iron with a rare earth element, neodymium, and boron, $Nd_2Fe_{14}B$, capable of generating at their surface the magnetic fields in excess of 1 T. They combine the desirable features of high magnetization (high remanence, up to 1.3 T), resistance to demagnetization (high coercivity, equivalent to more than 1 T), reasonably high Curie temperature (in excess of 300 °C, although their magnetization starts to degrade at much lower temperature, at around 150 °C), and a relatively low price (at around USD 100 per kilogram). Permanent magnets become indispensable for green energy technology development because they are a critical part of wind turbine generator (three metric tons of NdFeB magnets per megawatt) and became an important element of electric cars (in excess of 2 kg NdFeB per car). The NdFeB magnets are also a key part of a rapidly growing industry of unmanned aerial vehicles (UAVs) or drones. The predicted growth in the global use of the permanent magnets leads to concerns about the limited supply of rare earth metals and their becoming an element of strategic importance, leading to renewed interest in research and development of new permanent magnet materials not relying on rare earth metals.

The magnetization of the ferromagnetic materials is determined by the applied magnetic field and their magnetization history (hysteresis) (Fig. 1). In particular, pure metallic iron exhibits the highest saturation magnetization of all permanent magnet materials, $M_s = 2.17$ T. The corresponding effective magnetic dipole moment of iron atom in the elemental iron sample is 2.2 Bohr magnetons. Pure metallic iron is characterized by low saturating field, 15 mT, but also by a low coercivity, 4 mT, which makes it a "soft" magnetic material (easy to demagnetize, unsuitable for magnetic field generation in magnetic structures). It is a good conductor of magnetic flux (high magnetic permeability, $\mu \approx 10^6$) and as such it is a principal component of magnet pole pieces. In contrast, the permanent magnets such as NdFeB are designed for high coercivity (that makes them a "hard" magnetic material) as well as for high remanence, $M_s = 1.3$ T, and as such they are used to generate magnetic field in magnetic structures. The permanent magnet structures are often a combination of soft and hard magnetic materials engineered for optimal generation and conduction of magnetic fluxes, in analogy to Kirchhoff's electric circuit laws.

The second quadrant of the magnetization hysteresis curve is important in describing the properties of permanent magnets. A desirable feature of a

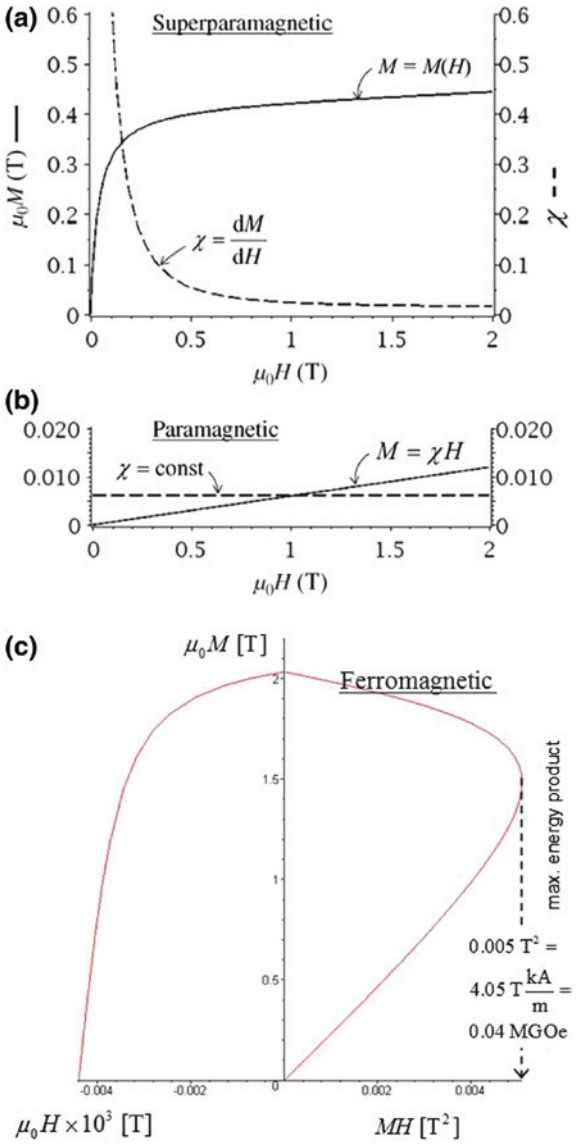

Fig. 1 Magnetization of paramagnetic and ferromagnetic materials. Note lack of hysteresis for paramagnetic materials and superparamagnetic iron oxide nanoparticles, SPIONs. **a** Magnetization M, and volume magnetic susceptibility, χ of the superparamagnetic particles (*top panel*) and **b** a paramagnetic compound (gadolinium chloride) as a function of the applied field H. The free space magnetic permeability constant μ_0 is used to convert units of M to tesla (T). Note differences in ordinate scales (same units as in panel a) and the differences in functional dependence on H between paramagnetic and superparamagnetic particles. **c** Second quadrant of the magnetic hysteresis loop (the demagnetization *curve*) and the corresponding plot of the magnetic energy product, $\mu_0 MH$, showing the maximum energy product of 0.04 MGOe used as a figure of merit for magnet comparison (adapted from Zborowski and Chalmers 2008, 2015, with permission)

permanent magnet is its high remanent magnetization, M_r, and high coercive force, H_c. A plot of the energy product, $\mu_0 M \times H$, for the second quadrant of the magnetization hysteresis loop (Fig. 1c) is used to determine the maximum energy product, a figure of merit when comparing different permanent magnet materials. It is approximately equal to 10 MGOe (mega–gauss–oersted, or 10^6 G × Oe) for Alnico magnets and over 50 MGOe for NdFeB magnets (Hatch and Stelter 2001).

The area enclosed by the hysteresis loop on the *M–B* plot is equal to work expended on the material magnetization, to increase the boundaries of magnetic domains aligned with the field at the cost of contracting boundaries of the magnetic domains that are not, and to realign the atomic dipole moments. The work is dissipated in the form of heat. The large hysteresis of hard magnets, such as ferromagnetic micro- and nanoparticles, makes them an ideal material for application to local thermotherapy using oscillating magnetic field (Krishnan 2010).

The commercial availability of inexpensive, permanent magnets of different shapes and magnetization directions, protected from corrosion by nickel plating, provides unique opportunities for magnetic cell separation. They could be arranged in various configurations for high field [4 T, (Furlani 2001)] and high gradient (Osman et al. 2012) at microscale that makes them an ideal source of the magnetic field for cell separation purposes. Selected examples of such permanent magnet configurations are shown in Fig. 2.

4 Magnetophoresis

Magnetophoresis is a phenomenon of particle motion in viscous media induced by the applied magnetic field. It underlies magnetic cell separation processes relying on differential binding of magnetic label particles to cells. Because it involves motion of cells in aqueous suspensions, it belongs to a part of fluid dynamics that deals with the particle suspensions exposed to external forces, together with gravitational and electrical forces. It is governed by a balance between the local magnetic body forces and viscous stresses on a cell-magnetic label complex that determine the velocity of the labeled cells in suspension and thus the efficiency of magnetic cell separation. The typical approach to describing such particle dynamics is to consider pertinent time constants and characteristic dimensionless numbers entering the equations of motion cell–label complex.

4.1 Cell Reynolds Number

The Reynolds number is a measure of inertial forces with respect to viscous forces and for a spherical cell in a fluid it is:

$$Re = \frac{\rho v D}{\eta}, \tag{13}$$

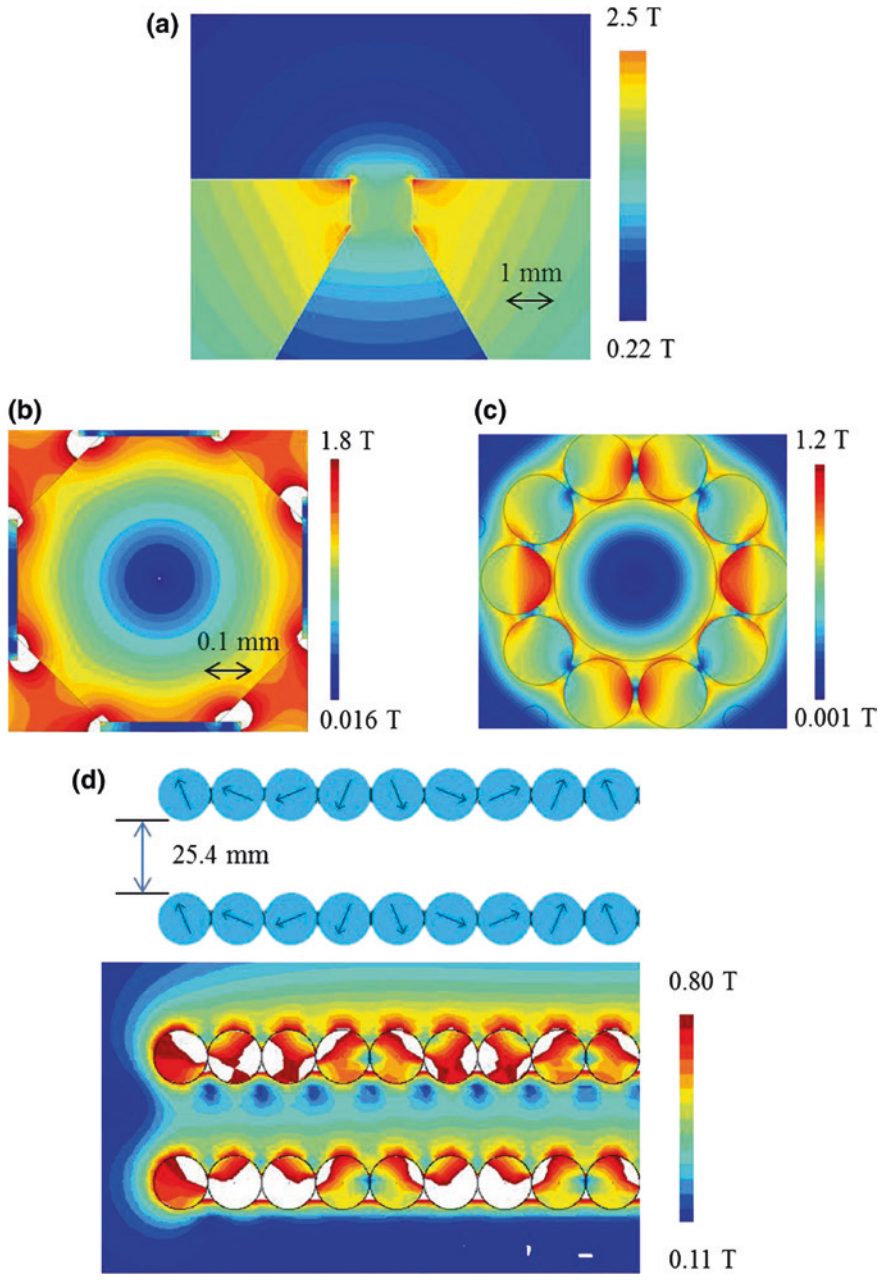

Fig. 2 Examples of permanent magnet configurations for generating high-field gradients. *Arrows* indicated magnetization direction. **a** Interpolar gap between two pentagons, **b** nearly quadrupole field between four rectangles, **c** circular Halbach array of cylindrical magnets magnetized diametrically in quadrupole configuration and **d** two linear Halbach arrays

where ρ is the fluid density, v is the cell velocity relative the bulk of the fluid, D is the cell diameter, and η is the fluid (dynamic) viscosity. For a white blood cell sedimentation in standard laboratory conditions, the representative values are $\rho \approx 1000\ \mathrm{kg/m^3}$, $D = 10\ \mu\mathrm{m} = 10^{-5}\ \mathrm{m}$, $v = 10^{-5}\ \mathrm{m/s}$ (one cell diameter per second), and $\eta = 10^{-3}\ \mathrm{Pa\ s}$ (at nearly 20 °C) resulting in the cell Reynolds number $Re = 10^{-4}$ and showing that the cell inertia is negligible in the description of cell sedimentation. For a (rigid) sphere the value of a critical Reynolds number above which the assumptions about the laminar fluid flow around the sphere do not apply is $Re = 10$. For a viscoelastic body, such as a cell, the onset of flow instabilities is at lower velocity and so critical $Re \approx 1$. Nevertheless, for typical cell diameters (<30 μm) considered in the magnetic cell separation, the cell Re numbers are well within the laminar flow model constraints, even for high cell velocities exceeding 1000 cell diameters per second (up to 30 mm/s). Such high velocities at microscale are possible with the use of SPIONs attached to cells and high magnetic field gradients, although the stress concentration at the point of the SPION attachment to the cell is likely to destroy it before it is reaching such high terminal velocities. In summary, the cell–SPION complex motion analysis under the influence of the applied magnetic field is based on assumptions of laminar flow conditions for typical separation conditions. The laminar flow assumptions apply to cell velocities in the range of several orders of magnitude.

4.2 Inertial Relaxation Time

The negligible inertial force relative to viscous force acting on cells in motion in aqueous media greatly simplify the equations of motion by reducing them to first-order differential equations of cell coordinates as a function of time. The length of time during which the inertial effects play a role is negligibly small and therefore can be omitted in the cell motion analysis:

$$\tau_\mathrm{p} = \frac{m_\mathrm{p}}{f} = \frac{\frac{\pi}{6}D^3\rho_\mathrm{p}}{3\pi\eta D} = \frac{\rho_\mathrm{p}D^2}{18\eta}, \tag{14}$$

where τ_p is the cell inertial relaxation time, m_p is the cell mass, $f = 3\pi\eta D$ is the Stokes friction coefficient, ρ_p is the cell density, D is the cell diameter, and η is the fluid (dynamic) viscosity. Thus for the cell density comparable to that of the aqueous media, $\rho_\mathrm{p} \approx 1000\ \mathrm{kg/m^3}$ and the other parameters as quoted above, $\tau_\mathrm{p} = 5.6\ \mu\mathrm{s}$, which is orders of magnitude shorter than characteristic times involved in the magnetic cell separation, typically tens to hundreds of seconds.

4.3 Stokes Flow

For the cell laminar motion, the viscous drag exerted on a spherical cell is directly proportional to its velocity relative to the bulk fluid:

$$F_{\mathrm{d}} = fv = 3\pi\eta D v, \tag{15}$$

where as before, f is the Stokes friction coefficient, η is the fluid (dynamic) viscosity, D is the cell diameter, and v is the cell velocity relative the bulk of the fluid. The viscous drag is the local reaction force of the viscous media (fluid) to the cell motion imposed by the applied field. Again, taking cell sedimentation as the simplest example of such a motion, the applied field is the difference between the cell weight and its buoyancy:

$$F_{\mathrm{g}} = \frac{\pi}{6} D^3 \left(\rho_{\mathrm{p}} - \rho_{\mathrm{s}}\right) g, \tag{16}$$

where D is the cell diameter, ρ_{p} and ρ_{s} are the cell and the fluid densities, respectively, and $g = 9.81\ \mathrm{m/s^2}$ is the standard gravitational acceleration. Due to the low cell *Re* number and the negligible effect of cell inertia on its sedimentation, Newton's second law of motion takes the form:

$$0 = F_{\mathrm{g}} - F_{\mathrm{d}}, \tag{17}$$

where the minus sign indicates that the drag force is opposed to the applied force, F_{g}. Combining Eqs. (14)–(16) one obtains the cell sedimentation velocity:

$$v = \frac{D^2}{18} \frac{\left(\rho_{\mathrm{p}} - \rho_{\mathrm{s}}\right)}{\eta} g \tag{18}$$

For the white blood cell density of $\rho_{\mathrm{p}} \approx 1050\ \mathrm{kg/m^3}$ the difference in the cell density and that of the aqueous media is $\Delta\rho = \rho_{\mathrm{p}} - \rho_{\mathrm{s}} = 50\ \mathrm{kg/m^3}$ resulting in the sedimentation velocity of $v = 2.7\ \mu\mathrm{m/s}$ or less than one third of the cell diameter per second.

4.4 Cell Sedimentation Coefficient

The ratio of the cell sedimentation terminal velocity to the field acceleration (gravitational or centrifugal) is the cell sedimentation coefficient:

$$s = \frac{v_g}{g} = \frac{D^2\left(\rho_{\mathrm{p}} - \rho_{\mathrm{s}}\right)}{18\eta} \tag{19}$$

which has the dimension of time (compare with Eq. 14). For the centrifugal acceleration fields, the parameter g in the equation above and in Eq. (18) is substituted

by the multiples of the standard gravitational acceleration ("number of g's"). For macromolecular centrifugal separations, the sedimentation coefficient is often quoted in the units of svedbergs, or S, where $1\ S = 10^{-13}$ s. For a representative white blood cell parameters, quoted above, the cell sedimentation coefficient is $s = 0.28\ \mu s$, or $2.8 \times 10^6\ S$. The sedimentation coefficient normalizes the sedimentation velocity of a cell by the acceleration applied to it. It is not dependent on the acceleration but only on the properties of the cell and the media.

4.5 Magnetophoretic Mobility

If the same fluid dynamic model as described above is applied to the cell motion in the magnetic field, then in the absence of gravitational effects, the magnetic field-induced cell velocity is obtained by substituting F_m, Eq. (3), for F_g in Eq. (17), leading to a magnetic analogue of Eq. (18):

$$v_m = \frac{D^2}{18} = \frac{(\chi_p - \chi_s)}{\eta} H \frac{dB}{dx} \tag{20}$$

where the densities of the cell and the fluid were replaced by their volume magnetic susceptibilities, χ_p and χ_s, respectively, and the gravitational field acceleration, g, was replaced by the magnetic field energy density gradient, $H\frac{dB}{dx}$. For the labeled cell–particle complex, the mean magnetic susceptibility of such a complex is much higher than that of the suspending media, which is unlike that for their respective densities, whose difference is small. The resulting magnetic field-induced velocities could be quite high, tens to hundreds cell diameter per second. Such high magnetic field-induced velocities are comparable to cell sedimentation velocities in high centrifugal fields of hundreds of g's.

The magnetophoretic mobility of a cell is its field-induced velocity normalized to the magnetic energy density gradient applied to it:

$$m = \frac{v_m}{H\frac{dB}{dx}} = \frac{D^2}{18} \frac{(\chi_p - \chi_s)}{\eta} \tag{21}$$

For linearly magnetizable media, the magnetophoretic mobility is not dependent on the magnetic field but only on the properties of the cell and the media (similar to the property of the sedimentation coefficient). Unlike the sedimentation coefficient, however, the magnetophoretic mobility is dependent on the field for nonlinear magnetic media, such as superparamagnetic particles and ferrofluids, for which the volume magnetic susceptibility is strongly dependent on the applied field, $\chi = \chi(H)$ (Fig. 1).

A particularly instructive way of characterizing the cell magnetophoresis is by normalizing the magnetic field-induced velocity, v_m, to the sedimentation velocity:

$$\frac{v_{\mathrm{m}}}{v_{\mathrm{g}}} = \frac{\chi_{\mathrm{p}} - \chi_{\mathrm{s}}}{\rho_{\mathrm{p}} - \rho_{\mathrm{s}}} \frac{H\frac{\mathrm{d}B}{\mathrm{d}x}}{g} \equiv \frac{\chi_{\mathrm{p}} - \chi_{\mathrm{s}}}{\rho_{\mathrm{p}} - \rho_{\mathrm{s}}} \frac{S_{\mathrm{m}}}{g} \tag{22}$$

where the symbol $S_m \equiv H\frac{\mathrm{d}B}{\mathrm{d}x}$ is introduced to simplify notation. Thus the dimensionless parameter $v_{\mathrm{m}}/v_{\mathrm{g}}$ describes the effect of the magnetic field on the field-induced cell velocity as a product of two factors: one dependent on the material properties of the cell and the fluid media only, $\frac{\chi_{\mathrm{p}}-\chi_{\mathrm{s}}}{\rho_{\mathrm{p}}-\rho_{\mathrm{s}}}$ and the other dependent on the applied field only, $\frac{S_{\mathrm{m}}}{g}$. For linearly magnetizable materials such separation of variables is exact but not for ferromagnetic and superparamagnetic materials whose magnetization saturates with the applied magnetic field and consequently, the magnetic susceptibility strongly depends on the applied field.

The use of Eq. (22) is illustrated here by comparing the magnetic cell separation to the centrifugal cell separation, a standard separation technique in biology laboratory. For practical purposes, centrifugal acceleration in laboratory centrifuges is quoted in multiples of the standard gravitational acceleration, or "number of g's". In typical laboratory applications, such as red blood cell (RBC) separation from whole blood, the centrifugal field is from 300 to 400 g applied for 15 and 5 min, respectively. Given that one measures the effectiveness of a separation technology by the time of separation, itself being inversely proportional to the field-induced velocity, inspection of Eq. (22) allows one to directly compare the effectiveness of magnetic separation with that of the centrifugal separation. For example, the density difference between a RBC and typical suspending buffer is $\rho_{\mathrm{p}} - \rho_{\mathrm{s}} = 84\ \mathrm{kg/m^3}$, whereas the difference in the volume magnetic susceptibility between a deoxygenated RBC and suspending buffer is on the order of $\chi_{\mathrm{p}} - \chi_{\mathrm{s}} = 5 \times 10^{-6}$ resulting in $\frac{\chi_{\mathrm{p}}-\chi_{\mathrm{s}}}{\rho_{\mathrm{p}}-\rho_{\mathrm{s}}} \approx 6 \times 10^{-8}\ \mathrm{m^3/kg}$. This indicates that in order to produce the magnetic field-induced velocity of the RBC comparable to its sedimentation velocity, $\frac{v_{\mathrm{m}}}{v_{\mathrm{g}}} \approx 1$ the magnetic field gradient to the gravity ($g = 9.81\ \mathrm{m/s^2}$) ratio should be $S_{\mathrm{m}}/g \approx 1.7 \times 10^7\ \mathrm{kg/m^3}$ or $S_{\mathrm{m}} \approx 1.7 \times 10^8\ \mathrm{N/m^3} = 1.7 \times 10^8\ \mathrm{A\,T/m^2}$, equivalent to $207\ \mathrm{T^2/m}$ (because $1\ \mathrm{T} = 1/\mu_0\ \mathrm{A/m} = 1/4\pi \times 10^7\ \mathrm{A/m}$). Considering that $S_{\mathrm{m}} = H\frac{\mathrm{d}B}{\mathrm{d}x} = \frac{1}{2\mu_0}\frac{\mathrm{d}B^2}{\mathrm{d}x}$, the required field gradient in the units of tesla is $2 \times 207\ \mathrm{T^2/m} = 417\ \mathrm{T^2/m}$. The advanced permanent magnet designs used for cell separation are capable of generating $S_{\mathrm{m}} \approx 10^9\ \mathrm{T\,A/m^2}$ (equivalent to $2500\ \mathrm{T^2/m}$) and therefore capable of producing RBC velocity up to six times its sedimentation velocity, thus equivalent to "6 g". This is obviously much lower than the centrifugal acceleration in laboratory centrifuges, by a factor of ~60. The resulting time of the RBC separation would be that much longer if performed over the separation distance equal to the height of the centrifuge tube (10 cm) and therefore quite unrealistic for such applications. Magnetic RBC separation is feasible in thin microfluidics channels, however, where the RBC separation travel distance (typically 250 μm) and thus the separation time can be substantially shortened (by a factor as high as 400) and made comparable to that of the RBC centrifugation.

Binding of SPIONs to cells greatly increases the cell–label magnetic susceptibility contrast relative to the fluid media, $\chi_{\mathrm{p}} - \chi_{\mathrm{s}}$ by up to several order of magnitudes. This results in high magnetic field-induced velocities, equivalent to "300 g" for even moderate field gradients. The limiting factor is the volume of the magnetic field available for the separation.

5 Single Cell Measurement of Magnetophoretic Mobility, Cell Tracking Velocimetry, CTV

The previous discussions have established a theoretical basis for magnetophoresis, and have further extended this introduction to magnetophoresis by normalizing magnetophoresis with sedimentation velocity (Eq. 22). Equation (22) strictly applies to cases of linearly magnetizable materials and as written, would only apply to the intrinsic magnetic susceptibility of a cell or particle, χ_p. Alternatively, cells targeted for separation are routinely labeled with an antibody conjugate to a SPION (i.e., an anti-CD3 antibody conjugated to a MACS® particle). If a submicron SPION is conjugated to a supramicron particle, even if on the order of 10,000 binding events occur, the change in the labeled cell diameter and density is such that Eq. (22) still holds except that the typically very high magnetic susceptibility of the SPION, relative to a cell, would require that the value of χ_p is governed by the relatively small volume of the SPIONs. However, in contrast, when micron sized magnetic microbeads are attached to cells through antibodies, the size and density of the cell microbead conjugate are more closely dictated by the properties of the microbead (e.g., an anti-CD3 antibody conjugated to a Dynabead®) (Zhang et al. 2005).

As with most biological systems, a distribution exists with respect to many cellular properties, be they cell size, magnetic susceptibility, or the number of cell surface markers targeted with antibody–SPION conjugate. Further, the affinity of an antibody for a cell/surface marker can vary from cell to cell as well as antibody clone to antibody clone. To optimize the magnetic manipulation and sorting of cells, it highly desirable to optimize, and characterize the intrinsic magnetic susceptibility of a cell or the magnetic susceptibility imparted to the cell through an antibody–SPION conjugate.

When a cell is labeled with a SPION, mathematically the magnetophoretic mobility has shown to be characterized by

$$m = \frac{\phi_p \beta \, \mathrm{ABC}}{3\pi \eta D_{\mathrm{cell}}} + m_{\mathrm{cell}}, \tag{23}$$

where

$$\phi_p = \left(\chi_p - \chi_f\right) V_p, \quad B < B_{\mathrm{sat}} \tag{24}$$

or

$$\phi_p = \left(\frac{\mu_0 M_{\mathrm{sat}}}{B} - \chi_f\right) V_p, \quad B \geq B_{\mathrm{sat}}, \tag{25}$$

where m_{cell} is the magnetophoretic mobility of the unlabeled cell ϕ_p is the particle–field interaction parameter (equivalent to the particle magnetic polarization), ABC is the antibody binding capacity of a cell, and β is the number of magnetic particles per ABC. As presented in Eqs. (24) and (25), the value of ϕ_p is dependent on whether the SPION becomes saturated (Chalmers et al. 2010).

A number of magnetometer devices exist to measure the magnetic susceptibility of materials, including a Gouy and Faraday balance, vibrating magnetometer, and the superconducting quantum interference device (SQUID). While accurate, these devices only provide bulk measurements of materials and particles, and reflecting this bulk average, are typically reported on a per mass basis. In contrast, Eqs. (22)–(23) are written with respect to a single cell or particle.

To exploit this characteristic, an instrument was developed, Cell Tracking Velocimetry, CTV, which tracks the movement of individual cells in a constant magnetic energy gradient, S_m. Figure 3 presents a schematic diagram of the system. Using digital imaging technology and particle tracking software, it is possible to track on the order of 100–1000 cells at a time and obtain the vertical (sedimentation) and horizontal (magnetic) velocity components of the tracked cells velocity, which correspond to v_m and v_g in Eq. (22). Figure 4 presents a computer screen shoot from an analysis using the CTV to measure the sedimentation and magnetically induced velocity of oxygenated and deoxygenated red blood cells, Fig. 4a, b, respectively. The while lines are computer generated, and correspond to the trajectory the specifically tracked cell has taken over a number of individual frames. The difference between the vertical line in Fig. 4a and the diagonal line in panel (b) corresponds to the constant magnetic energy gradient, S_m, which is operating on the cells in the horizontal, right to left direction. The ratio of these

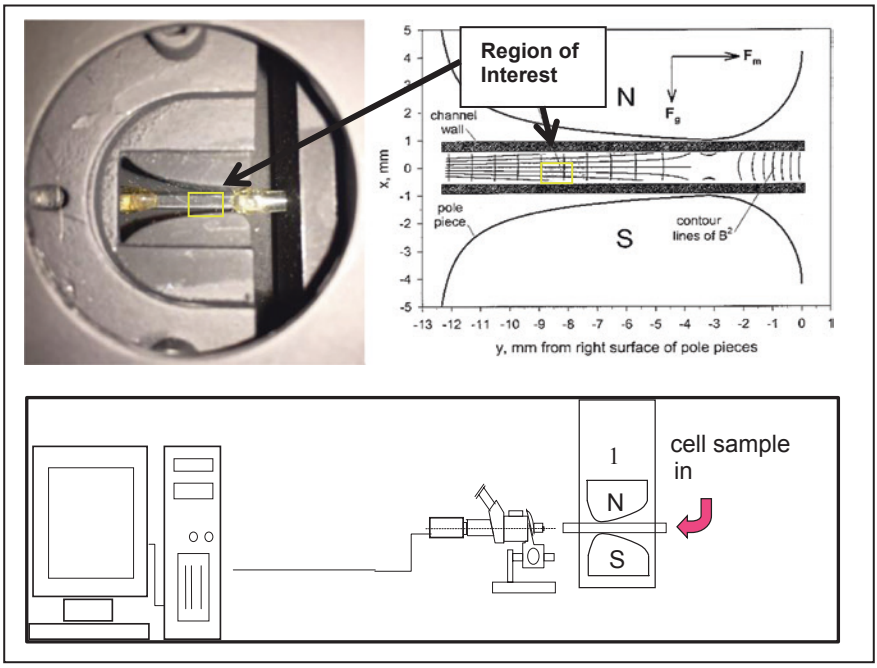

Fig. 3 Schematic diagram of cell tracking velocimetry (CTV) for measuring single-cell magnetophoretic mobility distribution in cell suspensions

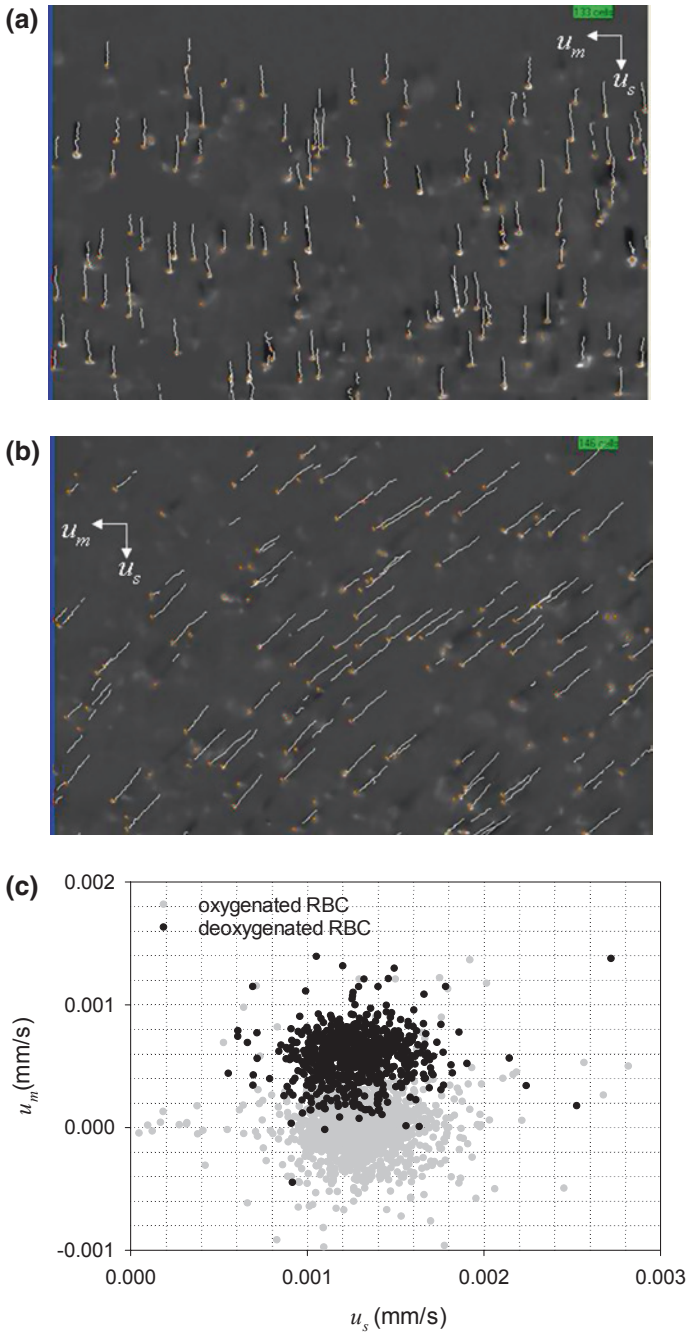

Fig. 4 Screenshots of CTC algorithm of tracked cells. The *white lines* are computer-derived trajectories of the cell as it moves from frame to frame. Panel **a** corresponds to oxygenated human RBCs, while panel **b** corresponds to the same donor deoxygenated, RBCs. Panel **c** is *dot plot* of the oxygenated and deoxygenated RBCs plotting magnetic versus settling velocity

Table 2 Mean volume magnetic susceptibility ($\chi = \mu_0 M/B$, at $B \approx 1$ T) and magnetic polarization (field–particle interaction parameter, $\phi = \chi V = \chi \pi D^3/6$) for selected commercial magnetic beads used for cell tagging (Zhang et al. 2005)

Magnetic beads	Lot nos.	$M_{s,nano\sim 0}/B$ (SI unit system)	Mean diameter (nm)	ϕ ($\times 10^{-25}$ m^3)
Streptavidin-MACS	5,020,305,031	$1.1 \pm 0.3 \times 10^{-3}$	116	8.8 ± 2.1
	5,030,918,049	$1.4 \pm 0.4 \times 10^{-3}$	67.2	2.3 ± 0.6
BD lmag	44,023	$1.4 \pm 0.3 \times 10^{-3}$	231	91 ± 20
Captivate	71 Al-1	$3.8 \pm 1.0 \times 10^{-4}$	136	5.1 ± 1.4
EasySep	2L226593	$3.5 \pm 1.2 \times 10^{-4}$	142	5.4 ± 2.0
	3A317176	$5.5 \pm 1.8 \times 10^{-5}$	160	12 ± 4

horizontal to vertical velocities corresponds directly to the ratio of velocities presented in Eq. (22). Figure 4c presents dot plots of the magnetically induced velocity versus the settling velocity of the oxygenated (gray dots) and the deoxygenated (black dots) of the RBCs presented in Fig. 4a, b.

Beyond measuring the intrinsic magnetization of RBCs, as presented above and in Fig. 4, the CTV system has been extensively used to measure the field interaction parameter, ϕ of a number of commercial SPIONS, (Table 2) as well as the magnetophoretic mobility of a number of different cell types labeled with commercial SPIONs. Figure 5 presents one example in which both the magnetophoretic mobility (and corresponding number of SPIONS) of labeled and unlabeled human lymphocytes when the CD3 surface marker is targeted.

6 Experimental and Theoretical Range of Magnetophoretic Mobility

Tracking the movement of cells, or particles as a result of the imparting of a magnetic force is surprising sensitive. Chalmers et al. (2010) reported that on the order of several hundred commercial SPIONs, nonspecifically bound to a cell can be measured. They further estimated that since a single cell can be tracked with the CTV system, and estimates can be made on the Fe content per SPION, the CTV system has sensitivity on the order of 4.6×10^{-15} g/mL. This compares favorably to an inductively coupled plasma mass spectrometer (ICP-MS), which has typical sensitivity for Fe on the order of 10^{-8} g/mL.

The operational scope of the CTV instrument, including physical and equipment constraints, such as Brownian motion, creeping flow, the diffraction barrier of microscope, wall effect of channel, and software restraints have been previously discussed (Xue 2016) and are summarized in Fig. 6.

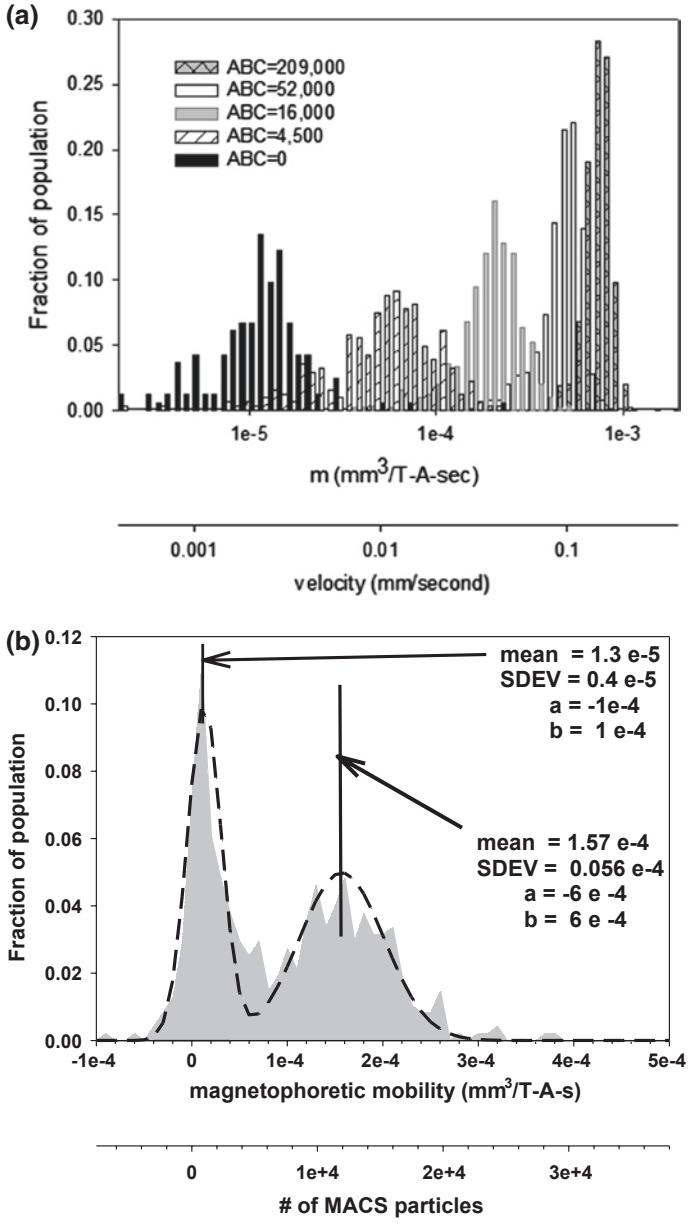

Fig. 5 **a** Histogram of the magnetophoretic mobility as a function of ABC for quantum simply cellular microbeads. These beads were labeled with MACS® Beads (McCloskey et al. 2000). **b** Magnetophoretic mobility of human peripheral blood leukocytes (PBL) labeled with anti-CD3-PE and anti-PE MACS particles. The labeling concentration was 40 μL for the anti-CD3-PE and five times the company recommended value for the anti-PE MACS (Lara et al. 2006)

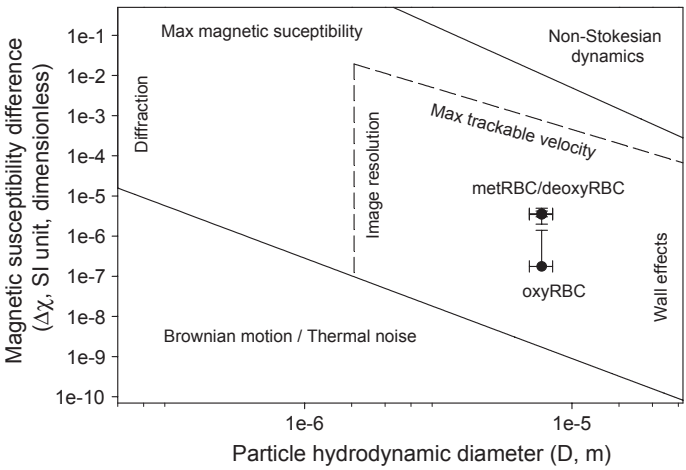

Fig. 6 Operational scope of the CTV approach. *Solid line* corresponds to physical limitation for the method and the *dashed line* presents the limitation for current setup. The result for oxygenated RBCs (oxyRBC), methemoglobin RBCs (metRBC) and deoxygenated RBCs (deoxy) are also shown (*error bar* as standard deviation). The metRBC and deoxyRBC results, which are essentially different, overlap in the figure due to the scale *vertical axis*. The oxyRBC magnetic susceptibility difference only shows upper error, due to the limitation of logarithmic scale of *vertical axis* (Xue 2016)

7 Examples of Various Geometries of Magnetostatic Energy Gradients in Application to Magnetic Cell Separation

7.1 High Gradient Magnetic Separator (HGMS)

The term and the abbreviation "HGMS" in the magnetic cell separation literature is typically limited to secondary effects of the magnetic field on ferromagnetic materials that induce high magnetic field gradients on small surface features of such materials (such as wires) (Watson 1973). Notable early applications include removal of weakly paramagnetic, iron oxide impurities from kaolin clays for high quality porcelain and paper production (Beharrell 2012) and for environmental water treatment, requiring high-field gradients for capture of weakly magnetic contaminants (Nishijima and Takeda 2006). They are particularly well suited for small-scale separation in biology. A primary example is MACS® separation system is based on disposable HGMS columns magnetized by insertion between pole pieces of a permanent magnet, and colloidal magnetic particles for cell labeling (Miltenyi et al. 1990). The columns are filled with a matrix of soft magnetic material in the shape of submillimeter diameter wires or spheres that generate high magnetic field gradient on their surfaces in the presence of the external magnetic field. The permanent magnet field approaches 1 T and the gradients up to 1000 T/m in the submillimeter

interstitial spaces of the magnetized matrix (Kantor et al. 1998). The matrix provides a highly developed surface for magnetic cell capture in the small volume of the column. Upon removal from the magnet, the matrix is demagnetized allowing release of the captured cellular material from the column. The MiniMACS® columns are only 7 mm in diameter and 50 mm long but are capable of separating up 10^6 labeled cells from a mixture of up to 10^7 cells in a volume of 1 mL in a matter of several minutes. The system has been developed over 25 years ago (Miltenyi Biotec GmbH, Bergisch Gladbach, Germany) and has diversified since into many different column and magnet sizes, selection of magnetic reagents and modes of operation, including an automated capture-and-release system (Grützkau and Radbruch 2010). The company provides a wide selection of the magnetic labeling reagents, including mouse monoclonal antibodies against major human cell clusters of differentiation (CD) and anti-mouse antibodies conjugated to magnetic beads for added versatility by the indirect magnetic labeling. It provides such staples of immunocytochemistry as avidin–biotin labeling reagents and fluorescence labeling reagents adapted to magnetic cell labeling (http://www.miltenyibiotec.com). The simplicity of operation and compatibility with the immunocytochemistry protocols contributed to its wide adoption in biology research and laboratory medicine. It has established the magnetic cell separation as one of the standard laboratory techniques, alongside centrifugation and fluorescence-activated cell sorting (FACS).

7.2 Open Gradient Magnetic Separator (OGMS)

The term describes a direct effect of the applied magnetic field on the separands not requiring ferromagnetic matrix inserts for separation and is occasionally used to differentiate it better from the HGMS principle of operation (Fukui et al. 2002). The advantages include independence of specialized, dedicated HGMS columns and thus greater flexibility in the choice of separation vessels and lower cost (Caralla et al. 2013; Joshi et al. 2015; http://www.easysep.com). The disadvantage is a relatively low magnetic field gradient, typically two orders of magnitude smaller than what is possible inside the HGMS column, which for the cell separation applications necessitates the use of more magnetic beads to achieve the same magnetic ponderomotive force acting on the cell–label complex. Such higher magnetic moment per bead is most readily achieved by increasing the magnetic bead size, as the magnetic moment increases with the third power of the bead diameter (with the other bead parameters held constant). The prime example of such a highly magnetic bead is Dynabead® manufactured in the range of diameters from 1 (MyOne™) to 4.5 μm (M450). Its high magnetic moment offers flexibility in the design of the magnetic separators which makes it a popular choice in applications to clinical diagnostic tests (Gijs et al. 2010; Ugelstad et al. 1993; https://www.thermofisher.com/us/en/home/brands/product-brand/dynal.html). Its relatively large surface area (as compared to the colloidal magnetic beads) makes it a suitable solid substrate for the molecular biology applications.

Apart from Dynabead brand, there is a large selection of superparamagnetic microbeads available on the market that are tailored to almost any specialized magnetic separation application of the OGMS type. They are often, but not always, sold together with dedicated magnet systems that are compatible with all typical biology laboratory containers, such as centrifuge tubes, multiwell plates, flasks, etc. (Gutierrez et al. 2015). Examples of the OGMS separators and dedicated magnetic microbeads include StemCell system (http://www.easysep.com) built around a multipole magnet in a cylindrical structure that fits 15 mL conical tubes and Becton Dickinson Immunosciences magnet rack (https://m.bdbiosciences.com/us/reagents/research/magnetic-cell-separation/other-species-cell-separation-reagents/cell-separation-magnet/p/55 2311) that fits six such tubes simultaneously.

7.3 Equilibrium Versus Steady-State Magnetic Separation

The majority of HGMS and OGMS systems described above operate in an equilibrium mode, in which the magnetic fraction is precipitated from the suspension on a suitable substrate surface and held there while the unseparated (nonmagnetic) fraction is removed and replaced with a clear solution. For a typical HGMS application (such as using Miltenyi MACS® system) the volumetric flow rate of the cell suspension through the HGMS column matches residence time necessary for the cell to reach the ferromagnetic matrix surface from the bulk suspension. For typical OGMS applications, the same is accomplished by letting the stationary cell suspension remain in the magnetic field for a sufficient length of time for all the magnetically labeled cells to travel to the vessel wall. Providing that the magnetic microbead saturation magnetization matches the available magnetic field and gradient, and the volume of the cell mixture is fully exposed to the magnetic field, such separations are accomplished quickly and with minimum intervention from the user. They are well suited for typical biological research laboratory protocols requiring small batches of cell suspensions (5–10 mL) and relatively small cell numbers (on the order of 10^8). For well-defined cell surface markers (such found in the CD library) and matching monoclonal antibodies (often available as ready-made cell labeling reagents from commercial companies) they are highly competitive in terms of specificity, cell viability, processing time, labor and equipment cost compared to alternative methods, such as sorting by flow cytometry (FACS).

The equilibrium mode operation of the HGMS and OGMS systems is dependent on the volume of cell batches required for separation, which is a limiting factor for large-scale cell separation, such as in application to cellular therapy. Such mode of operation is prone to the breakthrough effects due to the HGMS column overloading with the magnetically labeled cells, or the labeled cell losses in the wash fluid due to the limited cell access to the container wall surface inside the OGMS magnet. A solution is to either increase the physical dimensions of the

HGMS columns (Grützkau and Radbruch 2010) or the OGMS magnets (http://www.sepmag.eu/), or operate them in an intermittent fashion consisting of fill-capture-evacuate-wash cycles. An alternative approach is to redesign the system for a continuous flow operation with the magnetic cell fraction forming a continuous stream, split from the nonmagnetic fraction at the flow outlet (Pamme and Manz 2004; Hoyos et al. 2011). The first two approaches rely on the equilibrium mode separation and are basis of operation of large HGMS columns, automated HGMS systems for clinical applications [CliniMACS® line of products (http://www.miltenyibiotec.com)] and large OGMS flask systems (http://www.sepmag.eu/).

The continuous flow operation requires maintaining a dynamic equilibrium, or a steady state between the magnetic body forces and the viscous stress forces of the carrier solution acting on the cell–label complex in order to keep the magnetic cell complex in suspension, which brings additional elements of complexity to the system but also new opportunities of better separation (Takayasu et al. 2000). The general principle is described by the theory of field-flow fractionation (FFF) and its variant, split-flow thin (SPLITT) fractionation first developed in application to macromolecular separations using centrifugal, electric, and thermophoretic fields and subsequently extended to particulate suspension separations, including cell separation, by Giddings (1985) and Giddings et al. (Hoyos et al. 2011; Williams et al. 2010). The configuration of recent microfluidic channels is similar to that of a Hele–Shaw cell so that the separation dynamics can be reduced to a two-dimensional problem, whereby the applied magnetic forces are perpendicular to the advection forces resulting in spreading of the magnetically susceptible cell–label complexes across the flow width and their separation between multiple channel outflow ports (Lenshof and Laurell 2010).

The steady-state magnetic cell sorting in flowing suspensions include cell magnetophoretic fractionation according to the level of cell surface marker expression (Fig. 7) when used in combination with the colloidal magnetic labeling reagents (Schneider et al. 2010; Leigh et al. 2005; Adams et al. 2008), cell fractionation using magnetic repulsion in the magnetic susceptibility-modified carrier solutions (Watarai and Namba 2001; Moore et al. 2004; Peyman et al. 2009; Hwang et al. 1984; Tasoglu et al. 2015; Hahn and Park 2011) and a combination of magnetic and fluid dynamics inertial forces (Karabacak et al. 2014; Karle et al. 2010). The addition of fluid forces to the separation mechanism creates new opportunities for innovative design of magnetic elements (Adams et al. 2008; Gao et al. 2015) and a creative design of chemical reaction sequences on a cell–label complex crossing laminar streams of substrate solutions (Pamme 2012). The steady-state magnetic separation combined with a continuous flow operation offers the advantages of a large-scale separation (Doctor et al. 1986; Williams et al. 1999) without the added cost of the equipment scale-up and process automation, inherent to the equilibrium separation. The new opportunities of a better flow control in the microfluidics channels and matching magnetic field designs are being realized in numerous, innovative laboratory prototypes and commercial separators (Sahore and Fritsch 2014; Weston et al. 2010).

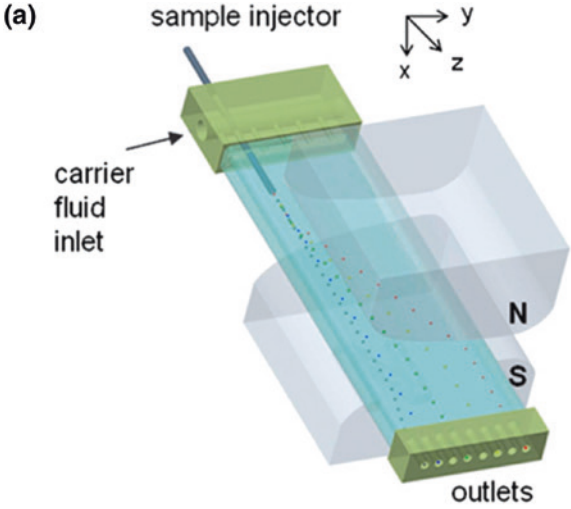
(a)
sample injector
y
x
z
carrier
fluid
inlet
N
S
outlets

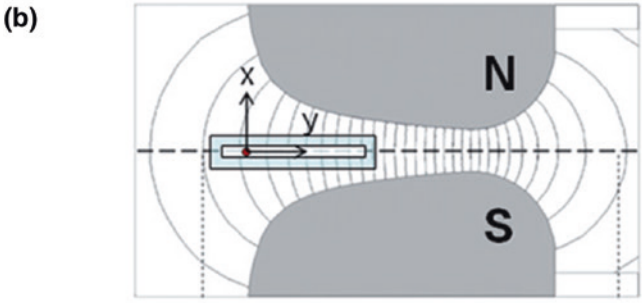
(b)
X
y
N
S

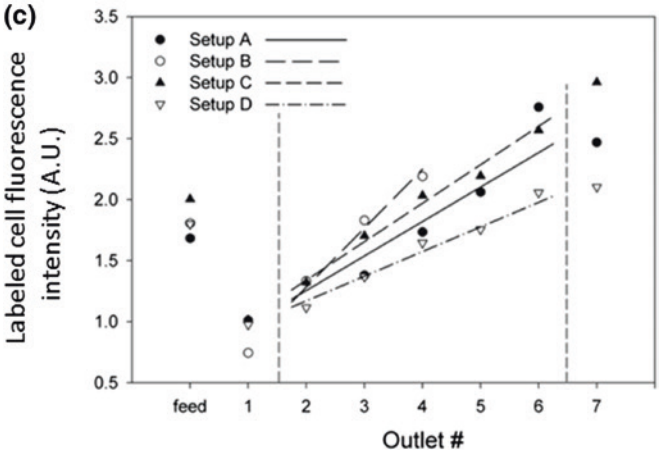
(c)
Labeled cell fluorescence intensity (A.U.)
3.5
3.0
2.5
2.0
1.5
1.0
0.5
Setup A
Setup B
Setup C
Setup D
feed
1
2
3
4
5
6
7
Outlet #

◀ **Fig. 7** **a** Principle of the dipole magnetic fractionator. The feed (cell suspension) is continuously injected into a carrier fluid flow inside a rectangular glass channel. The sample flows downward (z = direction) in the channel and is deflected from its flow path by an interaction with the magnetic field (y = direction) generated by a dipole magnet (not to scale). The sample is fractionated based on the strength of interaction with the magnetic field and collected in eight different outlet fractions. **b** Magnetic field lines inside the interpolar gap. **c** Labeled cell fluorescence intensity in arbitrary units (A.U.) for different cell fractions and different transport lamina distribution (for different outlet flow distribution setups *A–D*). Note the increase in the mean number of PE/cell with increasing outlet number as expected from the calculated values based on the cell surface marker expression and MM distribution in the unsorted sample in feed (adapted from Schneider et al. 2010, with permission)

8 Discrete Cell Manipulation, Label-Free Magnetic Separation and Other

Micromanipulation of cell-magnetic bead complexes using electric currents and microcoils fabricated using microelectromechnical systems (MEMS) techniques has been demonstrated (Shen et al. 2012; Ramadan et al. 2006). Innovative use of Halbach magnet arrays has been proposed for scale-up of connective tissue progenitor separation from bone marrow in applications to bone defect repair (Joshi et al. 2015) and to fractionation of disperse magnetic microbead suspensions (Ijiri et al. 2013).

Localization of high magnetic field gradients at the edges of small ferromagnetic features (such as wires) provides an opportunity for an exact control over cell-magnetic bead complex position and displacement at the microscale. This has been accomplished by micropatterning of thin layers of ferromagnetic material (such as nickel alloys) on silica substrates and application of external magnetic field. The ferromagnetic layer pattern provides means of creating a barrier to advection of magnetic bead–cell complexes in a fluid flow inside small channels and separation of such complexes from unlabeled cells (Fig. 8). Various combinations of ferromagnetic micropatterns and flow configurations have been proposed (Adams et al. 2008; Hu et al. 2015). Unlike separation in the HGMS columns (described above) the highly regular micropattern of the ferromagnetic layer and a well-defined, laminar flow in microchannels provide means of a better control over the cell-magnetic bead separation process. Innovative use of susceptibility-modified solutions for mass density difference-based separation and real-time imaging and analysis using smart phone has been demonstrated (Knowlton et al. 2015) (Fig. 9). The technology is particularly appealing in resource-poor settings. The application of magnetic separation for detection of malaria in asymptomatic children has been also demonstrated (Sumari et al. 2016) (Fig. 10).

Control over the domain magnetization of the ferromagnetic single-domain micropatterns provides additional level of precision in the magnetic bead positioning and translation. Because such domains behave like hard magnets and therefore their magnetization is independent of the applied field, this creates an opportunity for using both the attractive and repulsive forces between the single-domain and a

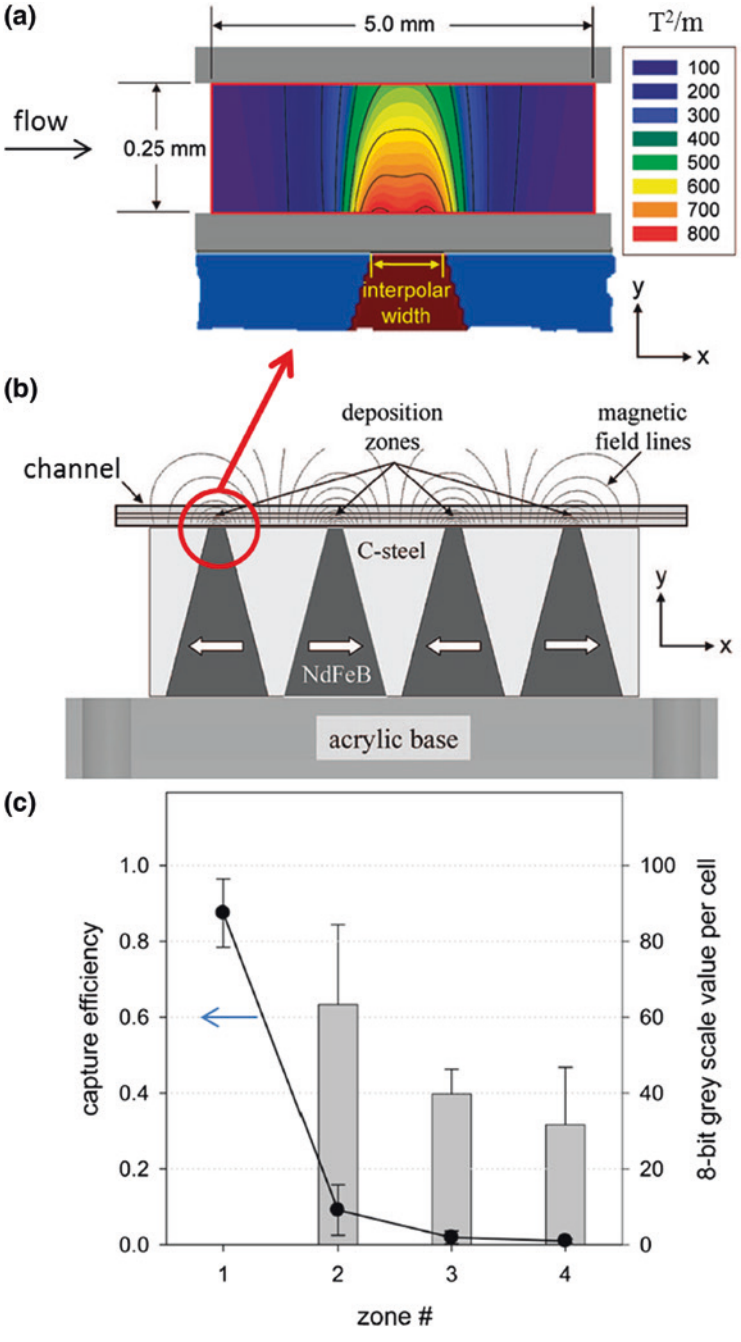
(a)
5.0 mm
T²/m
100
200
300
400
500
600
700
800
flow
0.25 mm
interpolar
width
y
x
(b)
deposition
zones
magnetic
field lines
channel
C-steel
NdFeB
acrylic base
y
x
(c)
capture efficiency
8-bit grey scale value per cell
1.0
0.8
0.6
0.4
0.2
0.0
100
80
60
40
20
0
1
2
3
4
zone #

◀ **Fig. 8** **a** Interpolar gap of a permanent magnet designed for an efficient capture of cell–label complex from a flowing suspension. The contour bands illustrate the magnitude of the *vertical* gradient component of magnetostatic potential energy (proportional to tesla^2/m, T^2/m). The gap width is 1 mm, channel height is exaggerated for clarity. **b** Four such interpolar gaps assembled together. The dimensional relationship between the parts is to scale. **c** Capture efficiency and fluorescence intensity (on a 8-bit gray scale) measured as a function of zone number. The *error bars* show one standard deviation from the mean for three experiments. Note capture of more fluorescent (and more magnetic) cells upstream from the channel outlet (adapted from Nath et al. 2009, with permission)

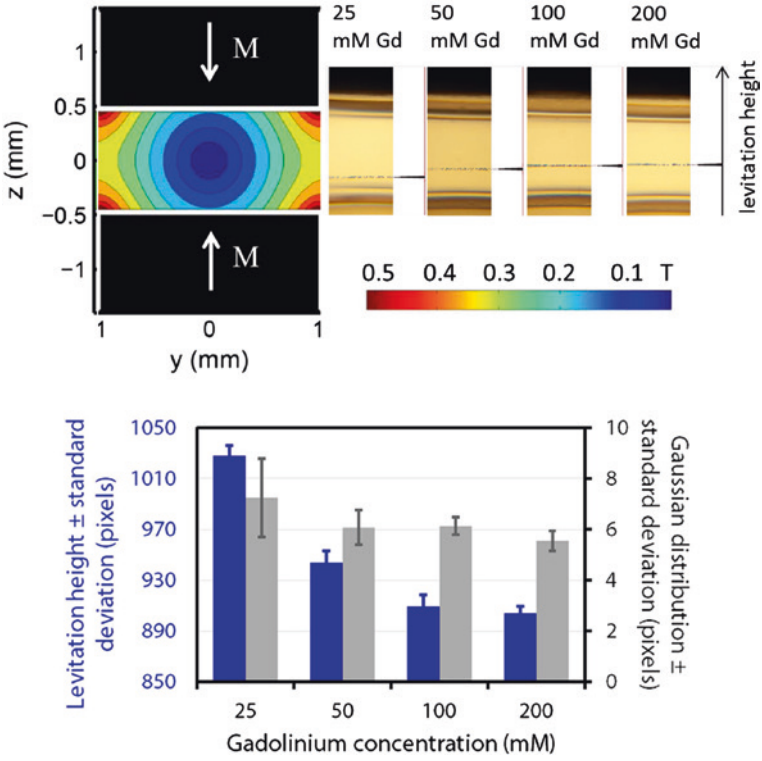

Fig. 9 Contour plot of the magnetic field between two, oppositely polarized permanent magnets. Images of levitating microspheres are acquired by the user with a smartphone fixed to the magnet and flow channel assembly and processed to determine the levitation height and confinement width of the microspheres in the sample stream, at different gadolinium concentration. (adapted from Knowlton et al. 2015, with permission)

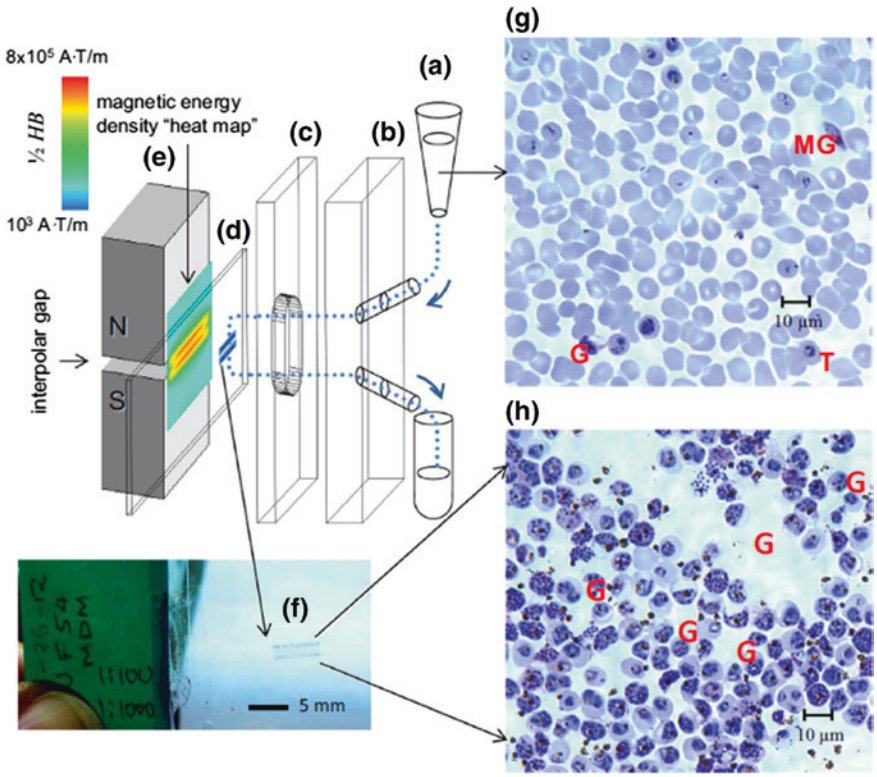

Fig. 10 Magnetic capture of malaria parasite infected red blood cells (RBCs) from RBC culture suspension. The cell suspension **a** is pumped through a channel comprising manifold platen with inlet and outlet ports (**b**), channel cutout spacer (**c**) and a transparent deposition slide (**d**), as indicated by *curved arrows*. The flow channel assembly **b**–**d** is pressed against the interpolar gap of a permanent magnet, **e** generating magnetic force on the magnetically susceptible cells due to a highly nonuniform fringing field, as indicated by the magnetic energy density map (*H* field in amperes per m, Å/m, and *B* field in tesla, T). The captured cells form a deposit **f** amenable to staining and microscopic analysis. **g** Shows approximately ×10 enrichment compared to the original sample, **h** NF54 strain, ×40 oil magnification) where *G* indicates gametocyte, *MG* male gametocyte, *T* trophozoite (adapted from Sumari et al. 2016, with permission)

superparamagnetic bead (type of a soft magnet) depending on the direction of the applied field. This has been demonstrated by superparamagnetic bead propulsion on a square grid of single-domain dots in a rotating magnetic field whereby the rotation of the induced magnetic dipole of the bead causes it to be sequentially pushed and pulled between the neighboring single-domain dots in synchrony with the rotating applied field vector (Hu et al. 2015; Chen et al. 2013). Increased bead capture rate is provided by generation of high-field gradients at the boundaries of magnetic domains (Fig. 11).

There are known, naturally occurring paramagnetic components of the cell that may become important for the label-free magnetic cell manipulation and

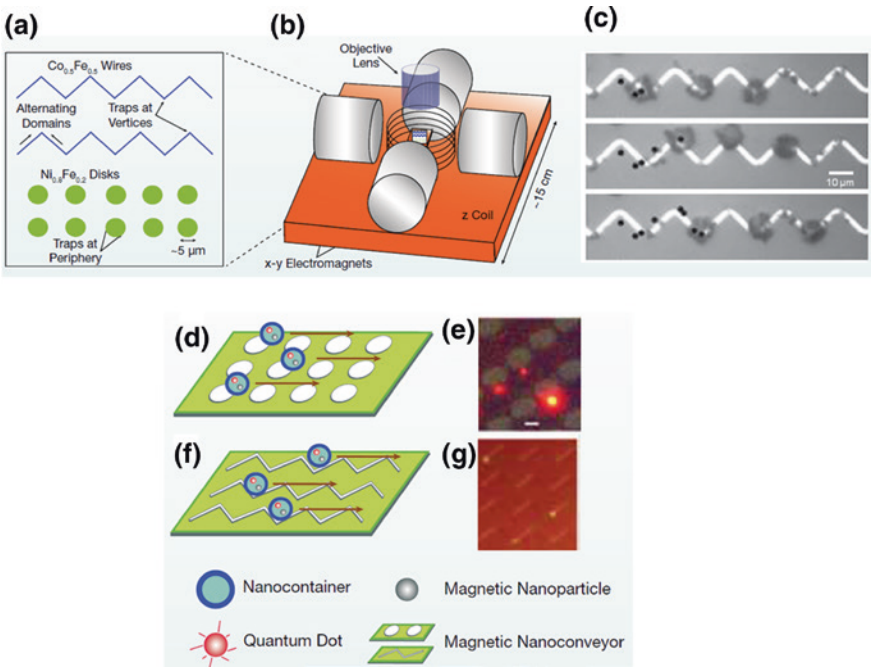

Fig. 11 The magnetic nanoconveyors shown in this schematic **a** are $Co_{0.5}Fe_{0.5}$ zigzag wires and $Ni_{0.2}Fe_{0.2}$ disks. *Points* on the periphery of a magnetized disk act as magnetic particle traps, whereas alternating magnetic domains in zigzag wires give rise to regions of high fields and field gradients at wire vertices. These regions act as traps for magnetic nanoparticles. The entire system, **b** including the external electromagnets and coil required to apply magnetic fields, can be mounted on an optical fluorescence microscope. Application of fields can strengthen, weaken, or move traps, allowing for manipulation of trapped entities along directed pathways. **c** T lymphocyte cells labeled with anti CD3 conjugated 1 µm magnetic particles are propagated along wires. **d** Nanoconveyor technology can be used to transport multiple individual nanocontainers, such as these that encapsulate fluorescent quantum dots for optical tracking and magnetic nanoparticles for controlled transport. **d**, **f** are schematics of nanocontainer transport on microfabricated disks and wire array conveyors, respectively. **e**, **g** Are superimposed differential interference contrast (DIC)/fluorescence images of fluorescent magnetic nanoparticle trapped on micropatterned disks (EF) and zigzag wire conveyors (**g**) (adapted from Mahajan et al. 2012, with permission)

separation given the increasing sophistication of the magnet and fluidics designs. An interesting example are magnetotactic bacteria that contain specialized organelles, magnetosomes, comprising magnetite crystals whose response to the vertical component of the geomagnetic field provide the sense of up-down direction, important for finding nutrients. This has been used to control the direction of a self-propelled motion of the magnetotactic bacteria using the magnetic field in laboratory conditions. A similar function of finding direction is attributed to the presence magnetite inclusions found in homing pigeons.

Other examples are related to the role of paramagnetic iron and manganese in cell biology, in particular as related to their being a part of a large family of

proteins collectively known as metalloproteins. These include an oxygen-carrying protein, hemoglobin, an iron storage protein, ferritin, electron transfer proteins, cytochromes, and superoxide dismutases (manganese). The interconversion between low-spin to high-spin hemoglobin during the binding and release of molecular oxygen has been studied by Pauling and Coryell (1936) as a part of the program of elucidating the nature of chemical bond by quantum mechanics. The increasing hemoglobin concentration in the course of red blood cell maturation was tested for mature erythrocytes enrichment from hematopoietic cell cultures (Jin et al. 2012). The feasibility of erythrocyte depletion from whole blood preparations as a type of a "magnetic centrifuge" was tested (Moore et al. 2013) and considered for application to depletion of aging erythrocytes from stored blood for blood banking purposes (Jin et al. 2011). The theory of magnetophoresis links the field-induced cell motion to the underlying molecular mechanisms (Zborowski et al. 2003; Jin et al. 2008). The feasibility of label-free magnetic cell separation in applications to intraerythrocytic malaria detection has been demonstrated in the laboratory (Hackett et al. 2009; Zimmerman et al. 2006) and tested in field studies (Sumari et al. 2016; Karl et al. 2008). The separation of bacterial spores rich in paramagnetic element manganese (Mn) has been demonstrated and their magnetophoretic mobility analyzed quantitatively (Melnik et al. 2007; Sun et al. 2011). The separation of green algae genetically modified for elevated expression of ferritin was compared with that of the wild type (Buck et al. 2015). A practical system using permanent magnets for field operation for detecting paramagnetic contaminants in food or environmental water has been proposed and tested (Mirica et al. 2010).

9 Conclusions

The field of the magnetic cell separation and manipulation is highly dynamic in response to rapid advances in single cell analysis and molecular biology assays, in nanomedicine and in microanalytical systems and lab-on-a-chip applications, as well as new opportunities created by microfluidics and nanofluidics. The increasing availability of strong permanent magnets and access to superconducting magnets and separators, combined with better understanding and control of fluid dynamical forces in microchannels open new directions for the future magnetic cell separation approaches, such as label-free magnetic separation based on differences in the paramagnetic contribution from natural components of the cell (metalloproteins) and diamagnetic cell separation. This chapter is just a snapshot of a rapidly evolving field and the reader is well advised to consult the latest information, also available online, if this presentation was successful in providing motivation for further study.

References

Adams JD, Kim U, Soh HT (2008) Multitarget magnetic activated cell sorter. Proc Natl Acad Sci USA 105(47):18165–18170. doi:10.1073/pnas.0809795105

Beharrell PA (2012) Applications of superconducting magnetic separation. Quantum Design, Inc., San Diego. http://www.qdusa.com/sitedocs/productBrochures/Applications_of_Superconducting_Magnetic_Separation_2012.pdf. Date Accessed 15 Mar 2016

Bozorth RM (1993) Ferromagnetism. Wiley-IEEE Press, London

Buck A, Moore LR, Lane CD, Kumar A, Stroff C, White N, Xue W, Chalmers JJ, Zborowski M (2015) Magnetic separation of algae genetically modified for increased intracellular iron uptake. J Magn Magn Mater 380:201–204. doi:10.1016/j.jmmm.2014.09.008

Caralla T, Joshi P, Fleury S, Luangphakdy V, Shinohara K, Pan H, Boehm C, Vasanji A, Hefferan TE, Walker E, Yaszemski M, Hascall V, Zborowski M, Muschler GF (2013) In vivo transplantation of autogenous marrow-derived cells following rapid intraoperative magnetic separation based on hyaluronan to augment bone regeneration. Tissue Eng Part A 19(1–2):125–134. doi:10.1089/ten.tea.2011.0622

Chalmers JJ, Xiong Y, Jin X, Shao M, Tong X, Farag S, Zborowski M (2010) Quantification of non-specific binding of magnetic micro- and nanoparticles using cell tracking velocimetry: implication for magnetic cell separation and detection. Biotechnol Bioeng 105(6):1078–1093. doi:10.1002/bit.22635

Chen A, Byvank T, Chang WJ, Bharde A, Vieira G, Miller BL, Chalmers JJ, Bashir R, Sooryakumar R (2013) On-chip magnetic separation and encapsulation of cells in droplets. Lab Chip 13(6):1172–1181. doi:10.1039/c2lc41201b

de Wit S, van Dalum G, Lenferink AT, Tibbe AG, Hiltermann TJ, Groen HJ, van Rijn CJ, Terstappen LW (2015) The detection of EpCAM(+) and EpCAM(−) circulating tumor cells. Sci Rep 5:12270. doi:10.1038/srep12270

Doctor RD, Panchal CB, Swietlik CE (1986) A model of open-gradient magnetic separation for coal cleaning using a superconducting quadrupole field. AIChE Symp Ser 82:154–168

Fukui S, Nakajima H, Ozone A, Hayatsu M, Yamaguchi M, Sato T, Imaizumi H, Nishijima S, Watanabe T (2002) Study on open gradient magnetic separation using multiple magnetic field sources. IEEE Trans Appl Supercond 12(1):959–962. doi:10.1109/TASC.2002.1018559

Furlani EP (2001) Permanent magnet and electromechanical devices: materials, analysis, and applications. Academic Press, San Diego

Gao L, Ct Wyatt Shields, Johnson LM, Graves SW, Yellen BB, Lopez GP (2015) Two-dimensional spatial manipulation of microparticles in continuous flows in acoustofluidic systems. Biomicrofluidics 9(1):014105. doi:10.1063/1.4905875

Giddings JC (1985) Optimized field-flow fractionation system based on dual stream splitters. Anal Chem 57(4):945–947

Gider S, Awschalom DD, Douglas T, Mann S, Chaparala M (1995) Classical and quantum magnetic phenomena in natural and artificial ferritin proteins. Science 268(5207):77–80

Gijs MA, Lacharme F, Lehmann U (2010) Microfluidic applications of magnetic particles for biological analysis and catalysis. Chem Rev 110(3):1518–1563. doi:10.1021/cr9001929

Grützkau A, Radbruch A (2010) Small but mighty: how the MACS®-technology based on nanosized superparamagnetic particles has helped to analyze the immune system within the last 20 years. Cytometry Part A 77A(7):643–647. doi:10.1002/cyto.a.20918

Gutierrez L, Costo R, Gruttner C, Westphal F, Gehrke N, Heinke D, Fornara A, Pankhurst QA, Johansson C, Veintemillas-Verdaguer S, Morales MP (2015) Synthesis methods to prepare single- and multi-core iron oxide nanoparticles for biomedical applications. Dalton Trans 44(7):2943–2952. doi:10.1039/c4dt03013c

Hackett S, Hamzah J, Davis TM, St Pierre TG (2009) Magnetic susceptibility of iron in malaria-infected red blood cells. Biochim Biophys Acta 1792(2):93–99

Hafeli UO, Aue J, Damani J (2008) The biocompatibility and toxicity of magnetic particles. In: Zborowski M, Chalmers JJ (eds) Magnetic cell separation. Elsevier B.V., Amsterdam

Hahn YK, Park JK (2011) Versatile immunoassays based on isomagnetophoresis. Lab Chip 11(12):2045–2048. doi:10.1039/c0lc00569j

Hatch GP, Stelter RE (2001) Magnetic design considerations for devices and particles used for biological high-gradient magnetic separation (HGMS) systems. J Magn Magn Mater 225(1–2):262–276. doi:10.1016/S0304-8853(00)01250-6

Hirota N, Kurashige M, Iwasaka M, Ikehata M, Uetake H, Takayama T, Nakamura H, Ikezoe Y, Ueno S, Kitazawa K (2004) Magneto-Archimedes separation and its application to the separation of biological materials. Phys B 346:267–271. doi:10.1016/j.physb.2004.01.063

Hoyos M, Moore L, Williams PS, Zborowski M (2011) The use of a linear Halbach array combined with a step-SPLITT channel for continuous sorting of magnetic species. J Magn Magn Mater 323(10):1384–1388. doi:10.1016/j.jmmm.2010.11.051

http://www.miltenyibiotec.com

http://www.easysep.com

http://www.sepmag.eu/. Last accessed April 2016

http://www.miltenyibiotec.com. Last accessed April 2016

https://m.bdbiosciences.com/us/reagents/research/magnetic-cell-separation/other-species-cell-separation-reagents/cell-separation-magnet/p/552311. Last accessed April 2016

https://www.thermofisher.com/us/en/home/brands/product-brand/dynal.html. Last accessed April 2016

Hu X, Abedini-Nassab R, Lim B, Yang Y, Howdyshell M, Sooryakumar R, Yellen BB, Kim C (2015) Dynamic trajectory analysis of superparamagnetic beads driven by on-chip micromagnets. J Appl Phys 118(20):203904. doi:10.1063/1.4936219

Hwang JY, Takayasu M, Friedlaender FJ, Kullerud G (1984) Application of magnetic susceptibility gradients to magnetic separation. J Appl Phys 55(6):2592–2594

Ijiri Y, Poudel C, Williams PS, Moore LR, Orita T, Zborowski M (2013) Inverted linear Halbach array for separation of magnetic nanoparticles. IEEE Trans Magn 49(7):3449–3452. doi:10.1109/TMAG.2013.2244577

Jakubovics JP (1994) Magnetism and magnetic materials. Cambridge University Press, Cambridge

Jiles D (2016) Introduction to magnetism and magnetic materials, 3rd edn. CRC Press, Boca Raton

Jin X, Zhao Y, Richardson A, Moore L, Williams PS, Zborowski M, Chalmers JJ (2008) Differences in magnetically induced motion of diamagnetic, paramagnetic, and superparamagnetic microparticles detected by cell tracking velocimetry. Analyst 133(12):1767–1775. doi:10.1039/b802113a

Jin X, Yazer MH, Chalmers JJ, Zborowski M (2011) Quantification of changes in oxygen release from red blood cells as a function of age based on magnetic susceptibility measurements. Analyst 136(14):2996–3003

Jin X, Abbot S, Zhang X, Kang L, Voskinarian-Berse V, Zhao R, Kameneva MV, Moore LR, Chalmers JJ, Zborowski M (2012) Erythrocyte enrichment in hematopoietic progenitor cell cultures based on magnetic susceptibility of the hemoglobin. PLoS One 7(8):e39491

Joshi P, Williams PS, Moore LR, Caralla T, Boehm C, Muschler G, Zborowski M (2015) Circular Halbach array for fast magnetic separation of hyaluronan-expressing tissue progenitors. Anal Chem 87(19):9908–9915. doi:10.1021/acs.analchem.5b02431

Kantor AB, Gibbons I, Miltenyi S, Schmitz J (1998) Magnetic cell sorting with colloidal superparamagnetic particles. In: Recktenwald D, Radbruch A (eds) Cell separation methods and applications. Marcel Dekker, New York, pp 153–173

Karabacak NM, Spuhler PS, Fachin F, Lim EJ, Pai V, Ozkumur E, Martel JM, Kojic N, Smith K, Chen PI, Yang J, Hwang H, Morgan B, Trautwein J, Barber TA, Stott SL, Maheswaran S, Kapur R, Haber DA, Toner M (2014) Microfluidic, marker-free isolation of circulating tumor cells from blood samples. Nat Protoc 9(3):694–710. doi:10.1038/nprot.2014.044

Karl S, David M, Moore L, Grimberg BT, Michon P, Mueller I, Zborowski M, Zimmerman PA (2008) Enhanced detection of gametocytes by magnetic deposition microscopy predicts higher potential for *Plasmodium falciparum* transmission. Malar J 7:66

Karle M, Miwa J, Czilwik G, Auwarter V, Roth G, Zengerle R, von Stetten F (2010) Continuous microfluidic DNA extraction using phase-transfer magnetophoresis. Lab Chip 10(23):3284–3290. doi:10.1039/c0lc00129e

Knowlton SM, Sencan I, Aytar Y, Khoory J, Heeney MM, Ghiran IC, Tasoglu S (2015) Sickle cell detection using a smartphone. Sci Rep 5:15022. doi:10.1038/srep15022

Krishnan KM (2010) Biomedical nanomagnetics: a spin through possibilities in imaging, diagnostics, and therapy. IEEE Trans Magn 46(7):2523–2558. doi:10.1109/TMAG.2010.2046907

Krishnan KM (2016) Fundamentals and applications of magnetic materials. Oxford University Press, Oxford, UK

Lara O, Tong X, Zborowski M, Farag SS, Chalmers JJ (2006) Comparison of two technologies to deplete T cells from human blood samples. Biotechnol Bioeng 94(1):66–80. doi:10.1002/bit.20807

Leigh DR, Steinert S, Moore LR, Chalmers JJ, Zborowski M (2005) Cell tracking velocimetry as a tool for defining saturation binding of magnetically conjugated antibodies. Cytometry Part A J Int Soc Anal Cytol 66(2):103–108. doi:10.1002/cyto.a.20155

Lenshof A, Laurell T (2010) Continuous separation of cells and particles in microfluidic systems. Chem Soc Rev 39(3):1203–1217. doi:10.1039/b915999c

Mahajan KD, Vieira GB, Ruan G, Miller BL, Lustberg MB, Chalmers JJ, Sooryakumar R, Winter JO (2012) A MagDot-nanoconveyor assay detects and isolates molecular biomarkers. Chem Eng Prog 108:41–46

McCloskey KE, Chalmers JJ, Zborowski M (2000) Magnetophoretic mobilities correlate to antibody binding capacities. Cytometry 40(4):307–315

Melnik K, Sun J, Fleischman A, Roy S, Zborowski M, Chalmers JJ (2007) Quantification of magnetic susceptibility in several strains of *Bacillus* spores: implications for separation and detection. Biotechnol Bioeng 98(1):186–192. doi:10.1002/bit.21400

Miltenyi S, Muller W, Weichel W, Radbruch A (1990) High gradient magnetic cell separation with MACS. Cytometry 11(2):231–238. doi:10.1002/cyto.990110203

Mirica KA, Shevkoplyas SS, Phillips ST, Gupta M, Whitesides GM (2009) Measuring densities of solids and liquids using magnetic levitation: fundamentals. J Am Chem Soc 131(29):10049–10058. doi:10.1021/ja900920s

Mirica KA, Phillips ST, Mace CR, Whitesides GM (2010) Magnetic levitation in the analysis of foods and water. J Agric Food Chem 58(11):6565–6569. doi:10.1021/jf100377n

Moore LR, Milliron S, Williams PS, Chalmers JJ, Margel S, Zborowski M (2004) Control of magnetophoretic mobility by susceptibility-modified solutions as evaluated by cell tracking velocimetry and continuous magnetic sorting. Anal Chem 76(14):3899–3907. doi:10.1021/ac049910f

Moore LR, Nehl F, Dorn J, Chalmers JJ, Zborowski M (2013) Open gradient magnetic red blood cell sorter evaluation on model cell mixtures. IEEE Trans Magn 49(1):309–315. doi:10.1109/Tmag.2012.2225098

Nath P, Strelnik J, Vasanji A, Moore LR, Williams PS, Zborowski M, Roy S, Fleischman AJ (2009) Development of multistage magnetic deposition microscopy. Anal Chem 81(1):43–49. doi:10.1021/ac8010186

Nishijima S, Takeda S (2006) Superconducting high gradient magnetic separation for purification of wastewater from paper factory. IEEE Trans Appl Supercond 16(2):1142–1145. doi:10.1109/TASC.2006.871346

Osman O, Zanini LF, Frenea-Robin M, Dumas-Bouchiat F, Dempsey NM, Reyne G, Buret F, Haddour N (2012) Monitoring the endocytosis of magnetic nanoparticles by cells using permanent micro-flux sources. Biomed Microdev 14(5):947–954. doi:10.1007/s10544-012-9673-4

Pamme N (2012) On-chip bioanalysis with magnetic particles. Curr Opin Chem Biol 16(3–4):436–443. doi:10.1016/j.cbpa.2012.05.181

Pamme N, Manz A (2004) On-chip free-flow magnetophoresis: continuous flow separation of magnetic particles and agglomerates. Anal Chem 76(24):7250–7256. doi:10.1021/ac049183o

Pauling L, Coryell CD (1936) The magnetic properties and structure of hemoglobin, oxyhemoglobin and carbonmonoxyhemoglobin. Proc Natl Acad Sci USA 22(4):210–216

Peyman SA, Kwan EY, Margarson O, Iles A, Pamme N (2009) Diamagnetic repulsion—a versatile tool for label-free particle handling in microfluidic devices. J Chromatogr A 1216(52):9055–9062. doi:10.1016/j.chroma.2009.06.039

Posfai M, Lefevre CT, Trubitsyn D, Bazylinski DA, Frankel RB (2013) Phylogenetic significance of composition and crystal morphology of magnetosome minerals. Front Microbiol 4:344. doi:10.3389/fmicb.2013.00344

Ramadan Q, Samper V, Poenar DP, Yu C (2006) An integrated microfluidic platform for magnetic microbeads separation and confinement. Biosens Bioelectron 21(9):1693–1702. doi:10.1016/j.bios.2005.08.006

Ramsey NF (1990) Molecular beams. The international series of monographs on physics. Oxford University Press, Oxford

Rosensweig RE (1997) Ferrohydrodynamics. Dover, Mineola

Russell AP, Evans CH, Westcott VC (1987) Measurement of the susceptibility of paramagnetically labeled cells with paramagnetic solutions. Anal Biochem 164:181–189

Sahore V, Fritsch I (2014) Redox-magnetohydrodynamics, flat flow profile-guided enzyme assay detection: toward multiple, parallel analyses. Anal Chem 86(19):9405–9411. doi:10.1021/ac502014t

Schneider T, Karl S, Moore LR, Chalmers JJ, Williams PS, Zborowski M (2010) Sequential CD34 cell fractionation by magnetophoresis in a magnetic dipole flow sorter. Analyst 135(1):62–70. doi:10.1039/b908210g

Schwinger J, DeRaad LLJ, Milton KA, W-y Tsai (1998) Classical electrodynamics. Perseus Books, Reading

Shen F, Hwang H, Hahn YK, Park JK (2012) Label-free cell separation using a tunable magnetophoretic repulsion force. Anal Chem 84(7):3075–3081. doi:10.1021/ac201505j

Simon MD, Geim AK (2000) Diamagnetic levitation: flying frogs and floating magnets (invited). J Appl Phys 87:6200–6204

Sumari D, Grimberg BT, Blankenship D, Mugasa J, Mugittu K, Moore L, Gwakisa P, Zborowski M (2016) Application of magnetic cytosmear for the estimation of *Plasmodium falciparum* gametocyte density and detection of asexual stages in asymptomatic children. Malar J 15(1):113. doi:10.1186/s12936-016-1170-4

Sun JJ (1980) Methods and apparatus for separating particles using a magnetic barrier. U.S. Patent

Sun J, Zborowski M, Chalmers JJ (2011) Quantification of both the presence, and oxidation state, of Mn in *Bacillus atrophaeus* spores and its imparting of magnetic susceptibility to the spores. Biotechnol Bioeng 108(5):1119–1129

Takayasu M, Kelland DR, Minervini JV (2000) Continuous magnetic separation of blood components from whole blood. IEEE Trans Appl Supercond 10(1):927–930

Tasoglu S, Khoory JA, Tekin HC, Thomas C, Karnoub AE, Ghiran IC, Demirci U (2015) Levitational image cytometry with temporal resolution. Adv Mater 27(26):3901–3908. doi:10.1002/adma.201405660

Thanh NTK (2012) Magnetic nanoparticles: from fabrication to clinical applications. CRC Press, Boca Raton

Ugelstad J, Stenstad P, Kilaas L, Prestvik WS, Herje R, Berge A, Hornes E (1993) Monodisperse magnetic polymer particles. New biochemical and biomedical applications. Blood Purif 11(6):349–369

Vojtisek M, Tarn M, Hirota N, Pamme N (2012) Microfluidic devices in superconducting magnets: on-chip free-flow diamagnetophoresis of polymer particles and bubbles. Microfluid Nanofluid 13:625–635. doi:10.1007/s10404-012-0979-6

Vyas KN, Palfreyman JJ, Love DM, Mitrelias T, Barnes CH (2012) Magnetically labelled gold and epoxy bi-functional microcarriers for suspension based bioassay technologies. Lab Chip 12(24):5272–5278. doi:10.1039/c2lc41022b

Watarai H, Namba M (2001) Magnetophoretic behavior of single polystyrene particles in aqueous manganese(II) chloride. Anal Sci 17(10):1233–1236

Watson JHP (1973) Magnetic filtration. J Appl Phys 44(9):4209–4213. doi:10.1063/1.1662920
Weston MC, Gerner MD, Fritsch I (2010) Magnetic fields for fluid motion. Anal Chem 82(9):3411–3418. doi:10.1021/ac901783n
Williams PS, Zborowski M, Chalmers JJ (1999) Flow rate optimization for the quadrupole magnetic cell sorter. Anal Chem 71(17):3799–3807
Williams PS, Carpino F, Zborowski M (2010) Characterization of magnetic nanoparticles using programmed quadrupole magnetic. Philos Trans Ser A Math Phys Eng Sci 368(1927):4419–4437. doi:10.1098/rsta.2010.0133
Xue W (2016) Measurements of Cellular Intrinsic Magnetism with Cell Tracking Velocimetry and Separation with Magnetic Deposition Microscopy, Ph.D. Thesis, The Ohio State University
Yavuz CT, Prakash A, Mayo JT, Colvin VL (2009) Magnetic separations: from steel plants to biotechnology. Chem Eng Sci 64:2510–2521
Zborowski M, Chalmers JJ (2008) Magnetic cell separation, vol 32. Laboratory techniques in biochemistry and molecular biology, vol 32. Elsevier, B.V., Amsterdam
Zborowski M, Chalmers JJ (2015) Magnetophoresis: fundamentals and applications. Wiley Encycl Electr Electron Eng. doi:10.1002/047134608X.W8236
Zborowski M, Malchesky PS, Jan TF, Hall GS (1992) Quantitative separation of bacteria in saline solution using lanthanide Er(III) and a magnetic field. J Gen Microbiol 138(1):63–68. doi:10.1099/00221287-138-1-63
Zborowski M, Fuh CB, Green R, Sun L, Chalmers JJ (1995) Analytical magnetapheresis of ferritin-labeled lymphocytes. Anal Chem 67(20):3702–3712
Zborowski M, Ostera GR, Moore LR, Milliron S, Chalmers JJ, Schechter AN (2003) Red blood cell magnetophoresis. Biophys J 84(4):2638–2645. doi:10.1016/S0006-3495(03)75069-3
Zhang H, Moore LR, Zborowski M, Williams PS, Margel S, Chalmers JJ (2005) Establishment and implications of a characterization method for magnetic nanoparticle using cell tracking velocimetry and magnetic susceptibility modified solutions. Analyst 130(4):514–527. doi:10.1039/b412723d
Zimmels Y, Yaniv I (1976) Characterization of magnetic forces by means of suspended particles in paramagnetic solutions. IEEE Trans Magn 4:359–368
Zimmerman PA, Thomson JM, Fujioka H, Collins WE, Zborowski M (2006) Diagnosis of malaria by magnetic deposition microscopy. Am J Trop Med Hyg 74(4):568–572